A&A 466, 481–499 (2007)
DOI: 10.1051/0004-6361:20065980

Astronomy & Astrophysics

The highly obscured region around PKS 1343 – 601

I. Galactic interstellar extinctions using DENIS galaxy colours⋆

A. C. Schröder[1], G. A. Mamon[2,3], R. C. Kraan-Korteweg[4,5], and P. A. Woudt[5]

[1] Department of Physics & Astronomy, University of Leicester, University Road, Leicester LE1 7RH, UK
e-mail: acs@star.le.ac.uk
[2] Institut d'Astrophysique de Paris (UMR 7095: CNRS & Université Pierre & Marie Curie) 98 bis Bd Arago, 75014 Paris, France
[3] GEPI (UMR 8111: CNRS & Université Denis Diderot), Observatoire de Paris, 92195 Meudon, France
[4] Depto. de Astronomía, Univ. de Guanajuato, Ap. P. 144, Guanajuato, GTO 36000, Mexico
[5] Department of Astronomy, University of Cape Town, Private Bag X3, Rondebosch 7701, South Africa

Received 5 July 2006 / Accepted 10 January 2007

ABSTRACT

The highly obscured radio-bright galaxy PKS 1343 – 601 at Galactic coordinates of $(l, b) = (309\overset{\circ}{.}7, +1\overset{\circ}{.}8)$ has been suspected to mark the centre of a hitherto unknown cluster in the wider Great Attractor region. As such it presents an ideal region for a search of galaxies in the near-infrared (NIR) and an in-depth study of their colours as a function of extinction. A visual search of a ∼30 square-degree area centred on this radio galaxy on images of the NIR DENIS survey (*IJK*) revealed 83 galaxies (including two AGNs) and 39 possible candidates. Of these, 49 are also listed in the 2MASS Extended Source Catalog 2MASX. Taking the IRAS/DIRBE extinction values (Schlegel et al. 1998, ApJ, 500, 525) at face value, the absorption in the optical (A_B) ranges from $\sim 2^{\rm m}$ to over $100^{\rm m}$ across the Galactic Plane. Comparing the detections with other systematic surveys, we conclude that this search is highly complete up to the detection limits of the DENIS survey and certainly surpasses any automatic galaxy finding algorithm applied to crowded areas.
The NIR galaxy colours from the 7″ aperture were used as a probe to measure total Galactic extinction. A comparison with the IRAS/DIRBE Galactic reddening maps suggests that the IRAS/DIRBE values result in a slight overestimate of the true extinction at such low Galactic latitudes, the inferred extinction from the galaxy colours corresponds to about 87% of the IRAS/DIRBE extinctions. Although this determination still shows quite some scatter, it proves the usefulness of NIR surveys for calibrating the IRAS/DIRBE maps in the extinction range of about $2^{\rm m} \lesssim A_B \lesssim 12^{\rm m}$.

Key words. galaxies: clusters: general – galaxies: fundamental parameters – galaxies: photometry – dust, extinction

1. Introduction

Various extragalactic large-scale structures are hidden behind the dust and stars of the Milky Way, the so-called Zone of Avoidance (ZoA), resulting in a poor understanding of the dynamics of the nearby Universe; for a detailed overview see Kraan-Korteweg & Lahav (2000), Kraan-Korteweg (2005), and the conference proceedings "Nearby Large-Scale Structures and the Zone of Avoidance" (Fairall & Woudt 2005). The Great Attractor (GA), an extended mass overdensity in the nearby Universe, lies for instance close to the crossing of the Supergalactic plane and the Galactic plane. Its presence was inferred by the systematic large-scale flow of elliptical galaxies (Lynden-Bell et al. 1988). Applying the potential reconstruction method of the mass density field POTENT (Dekel 1994), Kolatt et al. (1995) found its centre at $(l, b, v) = (320°, 0°, 4000\ \mathrm{km\,s^{-1}})$.

Close to the potential well of the GA lies the cluster ACO 3627 $(l, b, v) = (325°, -7°, 4848\ \mathrm{km\,s^{-1}})$, also called the Norma cluster. A deep optical galaxy search (Woudt & Kraan-Korteweg 2001) revealed this cluster to be as massive and rich a cluster as the Coma cluster (Kraan-Korteweg et al. 1996; Woudt et al. 2005). It therefore most likely marks the centre of the potential well of the GA. However, the GA is an extended region of high galaxy density (about 40° × 40° on the sky, see Kolatt et al. 1995), and other clusters (rich and poor) may well contribute substantially to this mass overdensity. Identifying them is a challenge as the central part of the wider GA area lies behind the thickest dust layer of the Milky Way.

About 10° from the Norma cluster, at $(l, b) = (309\overset{\circ}{.}7, +1\overset{\circ}{.}8)$, lies the galaxy PKS 1343 – 601 with a recession velocity of 3872 $\mathrm{km\,s^{-1}}$ (West & Tarenghi 1989). Near-infrared (NIR) observations revealed PKS 1343 – 601 to be a giant elliptical galaxy, which often reside at the centre of galaxy clusters. It is also one of the brightest radio sources in the sky (McAdam 1991): its flux density is only surpassed by Cygnus A, Centaurus A, Virgo A, and Fornax A. Two of these four radio sources are situated at the centre of rich clusters, one in a smaller cluster, and one in a group of galaxies (Jones et al. 2001). This evidence motivated Kraan-Korteweg & Woudt (1999) to use different means to investigate whether PKS 1343 – 601 points to another cluster in the GA region. Such a cluster would have a considerable impact on the local velocity-field calculations.

Results are still controversial. A preliminary analysis of the systematic deep H I search for galaxies with the Parkes Multibeam receiver found a concentration of galaxies in redshift space around this radio galaxy (Kraan-Korteweg et al. 2005b). A deep NIR search (*JHK*) of half a degree radius and a deep *I*-band survey of 2 degrees around PKS 1343 – 601 (Nagayama et al. 2004; Kraan-Korteweg et al. 2005a, respectively) have revealed a distribution of galaxies consistent with a

⋆ Table 2 and Appendix B are only available in electronic form at http://www.aanda.org

(medium-sized) cluster around PKS 1343 – 601. X-ray observations with ASCA have only revealed diffuse emission from PKS 1343 – 601 itself (Tashiro et al. 1998; see also the discussion in Ebeling et al. 2002), which would rule out a rich cluster.

This paper presents the results of a search for galaxies based on the NIR DENIS survey (Epchtein et al. 1997) in a much larger but shallower area than the above ones. The advantages of using the NIR to search for galaxies in the ZoA are manifold: (i) the NIR is less affected by the foreground extinction than the optical (the extinction in the *K*-band is about 10% of the extinction in the *B*-band); (ii) the NIR is sensitive to early-type galaxies, which are tracers of massive groups and clusters (contrary to far-infrared and blind H I surveys); (iii) the NIR shows little confusion with Galactic objects such as young stellar objects and cool cirrus sources.

In pilot studies, we assessed the performance of the DENIS survey at low Galactic latitudes (Schröder et al. 1997; Kraan-Korteweg et al. 1998; Schröder et al. 1999; Mamon et al. 2001). We tested the potential of the DENIS survey to detect galaxies where optical and far-infrared surveys fail, i.e., at high foreground extinctions and in crowded regions; we established that the NIR colours of galaxies lead to values for the foreground extinction; and we cross-identified highly obscured galaxies detected in a blind H I search at $|b| < 5°$. Overall, both systematic NIR surveys DENIS (*IJK*; Paturel et al. 2003; Vauglin et al. 1999) and 2MASS (*JHK*; Skrutskie et al. 2006; Jarrett et al. 2000a) have proved their effectiveness in penetrating the ZoA (Jarrett et al. 2000b; Rousseau et al. 2000; Schröder et al. 2000) – as long as the star density does not exceed a certain value (Kraan-Korteweg & Jarrett 2005).

In the following, we will introduce the DENIS survey and the implication of extinction on galaxy counts in general (Sects. 2 and 3, respectively). We then describe the search area and the quality of the DENIS data (Sect. 4), and the methods of galaxy and parameter extraction (Sect. 5). The catalogue data are described in Sect. 6, Sect. 7 gives a detailed comparison with the data of other searches and catalogues in this area, and in Sect. 8 we investigate the extinction in this area using the derived NIR colours. Conclusions are presented in the final Sect. 9. Throughout the paper, we assume a Hubble constant of $H_0 = 70\ \mathrm{km\,s^{-1}\ Mpc^{-1}}$.

A second paper will provide a detailed discussion of the local environment of PKS 1343 – 601 using the local galaxy density, the velocity distribution, and the X-ray luminosity to assess its mass and contribution to the GA overdensity (Schröder & Mamon 2007, hereafter Paper II).

2. The DENIS survey

The DENIS survey (DEep Near-Infrared Survey of the southern sky) is a European joint program that simultaneously imaged the sky in the Gunn-*i* (0.82 μm, hereafter *I*), *J* (1.25 μm) and K_s (2.15 μm, hereafter *K*) passbands with a resolution of 1″ in *I* and 3″ in *J* and *K* (Epchtein 1997, 1998). The observations were carried out between 1995 and 2001 with the dedicated 1 m ESO telescope at La Silla (Chile). About 92% of the southern sky ($+2° \le \mathrm{Dec} \le -88°$) has been covered.

DENIS images have a field of view of $12' \times 12'$. Exposure times per field and band are 9 s. The observing mode consisted of step-and-stare scans of 180 images in declination, resulting in *strips* of $12' \times 30°$. The overlap region between images are 1′ on each side. Any given $12' \times 30°$ *slot* in the sky was usually observed once and, depending on the quality of the images and/or weather conditions of the previous observations, repeated.

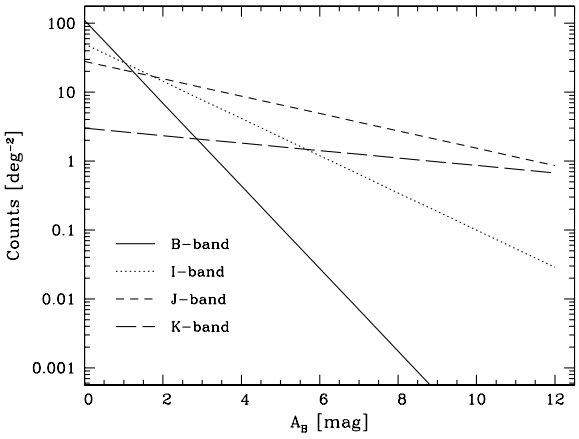

Fig. 1. Predicted galaxy counts in *B*, *I*, *J*, and *K* as a function of absorption in *B*, for highly complete and reliable DENIS galaxy samples and a $B_J \le 19^m$ optical sample.

The reduction process of the DENIS images consisted in bias corrections and flat-fielding. The latter was done using an iterative fitting of the pixel response over the night relative to the mean over the image centre (Borsenberger 1997). The images were then smoothed with kernels the size of which is a function of the wavelength of the spectral waveband. Objects were extracted and measured with `SExtractor` (Bertin & Arnouts 1996). For the purpose of the analysis of the ZoA the star/galaxy separation was, however, performed visually.

To ensure homogeneous quality over the whole survey, the DENIS processing centre in Paris (PDAC) recently re-processed all strips with the latest software of the pipeline. The limiting magnitudes for point sources (at a sensitivity of about 3σ) are $18\overset{m}{.}5$, $16\overset{m}{.}5$, $13\overset{m}{.}5$ for the *I*-, *J*-, and *K*-bands, respectively, while the completeness limits for galaxy extraction at high Galactic latitudes are roughly $16\overset{m}{.}5$, $14\overset{m}{.}8$, and $12\overset{m}{.}0$[1] (Mamon 1998, 2000).

3. Extinction effects on galaxy counts

In the ZoA, number counts of galaxies decrease due to the increasing foreground extinction. This effect depends, however, on wavelength. Using the formula given in Cardelli et al. (1989), the extinction in the DENIS NIR passbands are

$$A_I = 0.45A_B,\ \ A_J = 0.21A_B,\ \ A_K = 0.09A_B, \qquad (1)$$

directly implying that the decrease in number counts as a function of extinction will be considerably slower in the NIR than in the optical. Figure 1 shows the predicted surface number density of galaxies as a function of Galactic foreground extinction, using the DENIS *IJK* galaxy counts for their respective completeness limits as given in Mamon (1998), and for comparison the b_J galaxy counts of Gardner et al. (1996) in unobscured regions at the detection limit of $B_{\mathrm{lim}} = 19\overset{m}{.}0$ of the deep *B*-band search in this area (Woudt & Kraan-Korteweg 2001).

Figure 1 indicates that – given the above number counts and completeness limits – the NIR becomes more efficient at $A_B \gtrsim 2^m$ than the optical in revealing galaxies in the ZoA. The *J*-band seems the most efficient passband at intermediate extinctions ($2^m < A_B < 12^m$), whereas *K* becomes superior to *J* at $A_B \simeq 12^m$. As Kraan-Korteweg (2000) and

[1] The DENIS *K*-band limiting magnitude is bright because the *K* background of the DENIS camera is high and dominated by thermal emission of the instrument.

Table 1. DENIS strips in the searched area.

Slot	Strip	Date Obs.	RA (J2000)	Image Nrs	Bands	PSF (*IJK*)			Seeing	Weather	Astrom.	Prior.
(1)	(2)	(3)	(4)	(5)	(6)	(7)			(8)	(9)	(10)	(11)
4638	7641	02/04/99	13 28 00.1	1252 420 – 456	*IJK*	3.48	3.47	3.47	2	1	1	1
4639	7659	05/04/99	13 29 20.3	1256 423 – 459	*IJK*	2.73	3.10	3.32	1	1	1	1
4640	7652	04/04/99	13 30 40.1	1254 833 – 869	*IJK*	3.08	3.39	3.57	2	1	1	1
4640	9426	27/04/00	13 30 40.0	1631 704 – 740	*IJK*	2.62	3.14	3.15	1	4	1	2
4641	3625	03/03/96	13 31 60.0	435 889 – 925	*IJK*	2.89	3.07	3.33	1	1	1	1
4642	2018	10/03/95	13 33 04.9	151 274 – 310	*–JK*	–	–	–	–	–	–	3
4642	3823	02/04/96	13 33 20.0	476 115 – 151	*IJK*	2.91	3.85	3.43	2	1	1	2
4642	7747	18/04/99	13 33 20.1	1275 855 – 891	*IJK*	2.92	3.14	3.19	1	1	1	1
4643	3981	02/05/96	13 34 40.0	508 435 – 471	*IJK*	2.87	3.60	3.15	1	4	2	4
4643	9461	03/05/00	13 34 40.0	1638 871 – 907	*IJK*	3.68	3.93	3.96	3	1	1	2
4643	9523	18/05/00	13 34 40.0	1652 101 – 137	*IJK*	3.90	3.97	3.86	3	1	1	3
4643	10626	10/04/01	13 34 40.4	1889 552 – 588	*IJK*	2.88	3.20	3.26	1	1	1	1
4644	3586	25/02/96	13 35 60.0	428 563 – 599	*IJ–*	2.89	3.02	–	(1)	2	2	2
4644	6299	04/06/98	13 35 60.0	965 242 – 278	*I–K*	3.37	–	3.49	(2)	2	2	3
4644	6371	01/07/98	13 35 59.3	981 749 – 785	*IJK*	2.47	3.03	3.52	1	1	1	1
4645	7450	25/02/99	13 37 20.2	1209 560 – 596	*IJK*	3.50	3.59	3.36	3	1	1	2
4645	7462	27/02/99	13 37 19.9	1212 136 – 172	*IJK*	2.52	3.22	3.21	1	1	1	1
4646	3678	12/03/96	13 38 40.0	446 502 – 538	*IJK*	2.89	3.19	3.65	1	1	1	1
4647	7514	08/03/99	13 40 00.0	1223 679 – 715	*IJK*	3.07	3.31	3.29	1	1	1	1
4648	4145	03/06/96	13 41 20.0	542 355 – 391	*IJK*	2.73	3.11	3.24	1	1	1	1
4649	1970	27/02/95	13 42 23.1	142 790 – 826	*–JK*	–	3.09	3.55	–	–	–	3
4649	3737	21/03/96	13 42 39.2	458 518 – 554	*IJK*	2.90	3.94	3.27	1	1	1	1
4649	9418	26/04/00	13 42 40.0	1630 031 – 067	*IJK*	3.40	3.61	3.66	3	1	1	2
4650	2056	23/03/95	13 43 44.9	158 110 – 146	*–JK*	–	3.20	3.56	–	–	–	2
4650	6306	07/06/98	13 43 59.4	966 517 – 553	*IJK*	2.80	3.34	3.36	2	1	1	1
4651	4182	12/06/96	13 45 20.0	549 360 – 396	*IJK*	2.85	3.18	3.61	1	1	1	1
4652	7527	10/03/99	13 46 40.1	1226 594 – 630	*IJK*	2.92	3.03	3.14	(1)	1	2	1
4653	7532	11/03/99	13 48 00.0	1227 856 – 892	*IJK*	2.81	3.05	3.20	1	1	1	1
4654	7503	06/03/99	13 49 21.0	1221 263 – 299	*IJK*	3.00	3.16	3.25	2	1	1	1
4655	2019	10/03/95	13 50 24.2	151 478 – 514	*–JK*	–	2.91	3.10	–	–	–	2
4655	7497	05/03/99	13 50 40.6	1219 844 – 880	*IJK*	3.09	3.25	3.43	2	1	1	1
4656	7491	04/03/99	13 52 00.7	1218 448 – 484	*IJK*	3.35	3.46	3.53	2	1	1	1
4657	7484	03/03/99	13 53 20.1	1216 911 – 947	*IJK*	3.02	3.11	3.32	1	1	1	1
4658	6052	05/03/98	13 54 41.1	924 158 – 196	*IJK*	2.56	3.06	3.44	(1)	4	2	1
4659	5514	24/03/97	13 55 59.9	812 511 – 547	*IJK*	3.24	3.84	4.37	2	1	1	1
4660	4136	01/06/96	13 57 20.0	540 905 – 941	*IJK*	2.62	3.30	3.32	1	1	1	1
4661	3960	27/04/96	13 58 40.0	504 268 – 304	*IJK*	2.72	3.14	3.35	1	1	1	1
4662	3969	28/04/96	14 00 00.0	505 951 – 987	*IJK*	2.66	3.38	3.31	(1)	2	2	1
4663	5391	27/02/97	14 01 20.5	789 933 – 969	*IJK*	3.15	3.30	3.32	1	1	1	1
4664	3676	11/03/96	14 02 40.0	445 934 – 970	*IJK*	3.71	3.75	4.01	2	1	1	1
4665	3976	29/04/96	14 03 60.0	507 366 – 402	*IJK*	2.83	3.92	3.35	1	1	1	2
4665	8071	24/06/99	14 04 00.2	1345 712 – 748	*IJK*	3.42	3.72	3.75	3	1	1	1
4666	3952	26/04/96	14 05 20.0	502 766 – 802	*IJK*	2.48	3.28	3.29	1	1	1	1

Woudt & Kraan-Korteweg (2001) have shown, their diameter-limited ($D \geq 0\farcm2$) optical ZoA surveys start to become incomplete at $A_B \gtrsim 3^{\rm m}$. Here, the *J*- and *K*-bands will allow a much deeper penetration of the ZoA as long as the star density does not swamp the fields.

These are very rough predictions and do not take into account any dependence on morphological type, surface brightness (NIR surveys are for instance not very sensitive to late and/or low surface brightness spirals), orientation, and crowding, all of which may lower the number of actually detectable galaxies (e.g., Mamon 1994; Kraan-Korteweg & Jarrett 2005). One of the reasons we pursued this NIR in-depth study of galaxies behind the Milky Way was to investigate this further.

4. Characteristics of the DENIS data in the cluster area

The centre of our search area was put at the position of the giant elliptical PKS 1343 – 601 (RA = $13^{\rm h}46^{\rm m}57\fs5$, Dec = $-60°22'58''$, J2000). To assess whether the still to be identified galaxies form a cluster around PKS 1343 – 601, we have adopted a search radius that encompasses the equivalent of at least one Abell radius at the redshift distance of PKS 1343 – 601. The latter, defined as $r_{\rm Abell} = 1\farcm72/z$ (Abell 1958) where z is the redshift, is $r_{\rm Abell} = 2\fdg25$ for the radial velocity of $v \simeq 3900$ km s^{-1} (West & Tarenghi 1989) of the radio galaxy.

We have searched 29 DENIS slots of 37 images each. The total areal coverage amounts to ∼29.8 square degrees (cf. Fig. 3). Some of these slots have been observed more than once. In this case the best quality observation was selected for the visual examination, but coordinates and photometry were determined from all images that were of useful quality. Table 1 gives an overview of the observed slots and their characteristics.

Column 1: slot number (according to their designation in the sky).

Column 2: strip number (observations of a given slot with a unique number according to the observing date). Strip

numbers smaller than 3000 were part of the pre-survey (these have no *I*-band counterparts, and the exposure time was slightly larger); they were used for verification only since they are not astrometrically and photometrically calibrated.

Column 3: date of observation (DD/MM/YY).

Column 4: central Right Ascension of the strip (J2000) (recall that each image has a width of about 12′).

Column 5: image numbers for the searched area (only the last three digits are given for the final image).

Column 6: observed passbands.

Column 7: half-flux radius as calculated by `SExtractor` multiplied by 2 (an equivalent to the point-spread function, PSF). The half-flux radii were determined from all stars in the magnitude ranges $11\overset{\mathrm{m}}{.}0 < I < 15\overset{\mathrm{m}}{.}0$, $9\overset{\mathrm{m}}{.}0 < J < 13\overset{\mathrm{m}}{.}0$, and $7\overset{\mathrm{m}}{.}0 < K < 10\overset{\mathrm{m}}{.}5$ that do not lie within 50 pixels of the image border.

The entries in the table are the geometric means of the half-flux radii over the given images. The values are similar to, although in the *I*-band roughly 0.″7 greater than, the full width half maximum (FWHM) in arcseconds of the PSF calculated by PDAC. This is mainly due to the pixelization of the image.

Column 8: seeing quality as estimated from the photometry of stars (cf. Appendix A). 1 stands for good seeing (photometry not affected), 2 for medium seeing (7″-aperture photometry is affected), and 3 for bad seeing (all magnitudes affected). The numbers in brackets are an estimate of the seeing where the astrometry was insufficient for a statistical comparison of the photometry in the overlap regions.

Column 9: weather conditions. 1 indicates no clouds, 2 unknown conditions, 3 possible clouds, and 4 clouds.

Column 10: astrometric quality of the strips. The DENIS standard high accuracy of an rms of 0.″2 is indicated with a 1, lower accuracy with 2. For strips where astrometric calibration failed we determined the coordinates from the DSS[2]-red images (accuracy of about 2−3″).

Column 11: order of quality of strips with more than one observation (1 indicates the best strip, higher numbers designate lower priorities).

All priority 1 strips, except strip 6052, had photometric weather conditions. Lower quality images will have a systematic effect on the search results. It is unlikely to result in a loss of large galaxies, but in an increase of uncertain galaxies due to the blurring of faint stars into patches similar in appearance to small and faint galaxies. The photometry of galaxies obtained under adverse seeing conditions will obviously also have larger uncertainties.

5. Galaxy extraction and parameters

Extended objects ("nebulae") in general are either galaxies or objects of Galactic origin (typically emission or reflection nebulae). In crowded areas we also find many stars that are blended into elongated objects, or groups of (unresolved) faint stars that form a diffuse nebula-like patch. This is usually the main reason why automatic searches for galaxies, like `SExtractor`, fail at low latitudes. The sharp gradient in surface brightness with radius can be used to distinguish blended stars from galaxies. But if the stars are very faint and in addition the seeing condition is not very good, this criterion becomes less distinct even to the eye.

We have visually examined all the images. This was done with the DENIS visualisation package `Denis3d` by E. Copet. It is optimally suited to such a search for extended objects: apart from the full image in a given band, it simultaneously displays the *I*, *J*, and *K* zoomed-in images under the cursor. Using the zoom-windows each whole image was systematically scanned. The simultaneous inspection of an object in the 3 passbands facilitates the galaxy/star discrimination considerably as the relative appearance of highly-obscured galaxies in the three bands varies compared to stars (cf. Fig. 1). To ensure homogeneity of the search the same cut-values were applied to all images (min = −30 ADU and max = 70 ADU, conforming to values of typically −4.6 to 10.8σ in *I*, −6.9 to 16.0σ in *J*, and −4.4 to 10.2σ in *K*).

We compared our results closely to the deep *B*-band catalogue by Woudt & Kraan-Korteweg (2001, hereafter WKK; $B_{\mathrm{lim}} = 19\overset{\mathrm{m}}{.}0$), i.e., our initial list of candidates was cross-correlated with the *B*-band detections. We found that we had missed a few low surface brightness galaxies. These generally are very faint in the NIR, but we did recover them in hindsight. They were subsequently added to our list and classified as *BG*. Only one *B*-band galaxy was not visible in the NIR.

We also identified various extended Galactic objects; they are discussed in more detail in Sect. 6.2. When classification as a galaxy was not clear-cut, we labelled the object as an uncertain galaxy.

The automatic extraction package `SExtractor` (Bertin & Arnouts 1996) was used to derive *IJK* Kron-photometry for the visually detected galaxies. `SExtractor` computes total magnitudes ("best") as well as photometry in apertures of 3″, 5″, 7″, 10″, 20″, and 40″.

Colours were determined from the 7″-aperture magnitudes. This aperture was chosen to minimise contamination by superimposed stars on the one hand and the variation in seeing conditions on the other. Since the radial colour gradient is small in the NIR (e.g., Moriondo et al. 2001; Rembold et al. 2002), the effect of having different fractions of a galaxy within our fixed aperture will be small and will introduce less uncertainty in the colour than the increased star subtraction required for larger apertures.

By going back to the image, a careful analysis was made to test whether `SExtractor` has deblended all objects in the vicinity of the galaxy, and whether all the parameters agree with each other. As a result we give quality parameters for the photometry in each band, depending on whether the 7″-aperture and/or the total magnitude are estimated to be uncertain or unreliable.

Although `SExtractor` computes semi-major and semi-minor axes of an object, we have decided – for uniformity reasons – to derive the diameters by other means since not all our galaxies were extracted by `SExtractor` and some were contaminated by not-deblended stars. We employed the contour facility in `ds9` (Joye & Mandel 2003) to measure the semi-major axis $A_{\mathtt{ds9}}$ out to isophotes of $21\overset{\mathrm{m}}{.}75$, $20\overset{\mathrm{m}}{.}5$, and $18\overset{\mathrm{m}}{.}0$ in the *I*-, *J*-, and *K*-bands, respectively. The isophotes were selected to be quarter integers close to values where the DENIS images in the search area have similar noise characteristics.

To compare our diameters with the parameters calculated by `SExtractor` we used the isophotal area parameter `ISOAREA`:

$$A_{\mathrm{iso}} = \sqrt{\mathtt{ISOAREA}/\pi/(\mathtt{B}/\mathtt{A})},$$

which is typically 2`A` (with an rms of 1.″8). Figure 2 shows the residuals ($\log A_{\mathtt{ds9}} - \log A_{\mathtt{iso}}$) for each band. They agree well for *I* and *K*, while the *J*-band shows a small but significant deviation:

$$I\colon\ \Delta(\log A) = \ (0.04 \pm 0.07)\log A_{\mathrm{iso}} + 0.05 \pm 0.05$$
$$J\colon\ \Delta(\log A) = (-0.18 \pm 0.07)\log A_{\mathrm{iso}} + 0.20 \pm 0.06$$
$$K\colon\ \Delta(\log A) = \ (0.02 \pm 0.07)\log A_{\mathrm{iso}} + 0.03 \pm 0.04.$$

[2] The STScI Digitized Sky Survey.

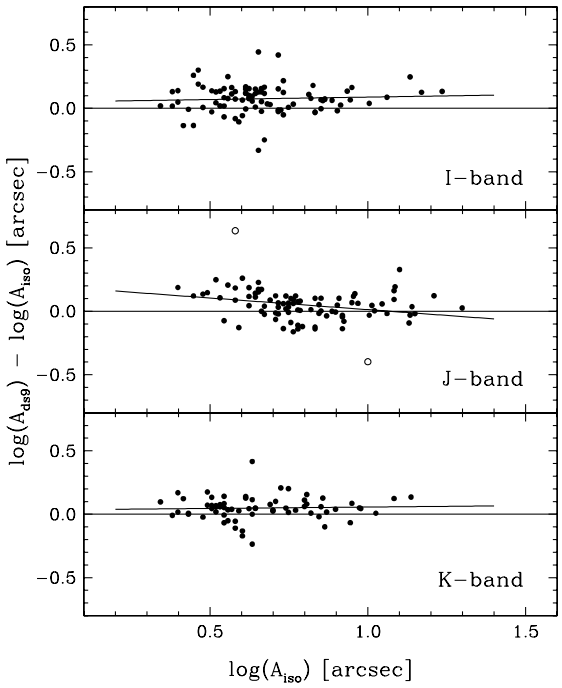

Fig. 2. The difference between the two estimates of the isophotal semi-major axis as determined with `ds9`, $A_{\rm ds9}$, and by `SExtractor`, $A_{\rm iso}$, is plotted versus the logarithm of $A_{\rm iso}$ for each passband. The least squares fit is plotted. *Open circles* (*middle panel*) indicate outliers removed in a second fit.

Two objects in the J-band fit show more than 3σ deviations from the fit. In both cases the object is partly blended with near-by stars which affects the automatic diameter extraction by `SExtractor`. If we exclude these outliers the fit will improve slightly to:

$$J:\ \log A_{\rm ds9} = (-0.12 \pm 0.06)\log A_{\rm iso} + 0.14 \pm 0.05.$$

These comparisons indicate that the isophotes of the semi-major axes derived with `ds9` agree well with the `SExtractor` limits in the I- and K-bands, whereas in the J-band `SExtractor` goes slightly fainter than $\mu_J = 20\overset{\rm m}{.}5$.

We have extracted magnitudes and diameters from all images where the respective object is visible (at a reasonable distance from the edge) and averaged those where the quality was acceptable.

We estimated the morphological types by visually inspecting all DENIS images as well as the DSS-red images. Fairly accurate classifications are possible at low extinctions (a comparison with the morphological types determined by WKK show good agreement). With increasing extinctions the outer spheroid becomes more and more truncated and a distinction between types more uncertain. At the highest extinction levels only the bulges of galaxies remain visible, making it impossible to distinguish between ellipticals and bulges of a spiral galaxies.

As a guide to the variation in dust content and the interpretation of the (absorbed) object parameters, the Galactic foreground extinctions have been determined from the IRAS/DIRBE maps by Schlegel et al. (1998). The colour excess $E(B-V)$ has been converted to A_B using $A_B = R_B\,E(B-V)$, where $R_B = R_V\,A_B/A_V$, $A_B/A_V = 1.337$ (Cardelli et al. 1989), and $R_V = 3.1$. Since the extinction maps were measured at 100 microns and converted to $E(B-V)$ using $R_V = 3.1$, the extinction values presented here are not very sensitive to an uncertainty in R_V. We present B-band extinction rather than I-band extinctions for easier comparison with other works in the ZoA.

Note that the IRAS/DIRBE extinction maps are not properly calibrated at latitudes $|b| < 5°$ and therefore only provide an estimate. In Sect. 8, a first attempt was made at calibrating the IRAS/DIRBE maps based on the reddened colours of the galaxies detected in this survey. Moreover, Schlegel et al. (1998) note in their paper that far-infrared point sources have been removed where source lists exists to correct for overestimates. This was not done for our search region, and we have taken care to check for possible point sources which could overestimate the local extinctions. No such source has been found in the search area.

Cameron (1990) has shown that to correct highly absorbed isophotal magnitudes of galaxies it is necessary to apply both a correction to the magnitude as well as a correction for the fact that the angular diameter of an obscured object appears smaller and therefore the isophotal magnitude appears fainter. Cameron has determined the correction for diameters in the optical B-band up to extinctions of $A_B = 6^{\rm m}$. The effect of extinction on the `SExtractor` Kron magnitudes is more difficult to estimate: the Kron "total" magnitude is the magnitude computed in an elliptical aperture aligned with the major axis found through the second moments but whose size is proportional to the first moment (Bertin & Arnouts 1996). The effect of extinction is to push the entire galaxy intensity profile down by some factor, which means that the detection isophote is smaller, hence the 1st order moment is smaller, meaning the Kron aperture is smaller, and the derived magnitude is fainter.

To analyse this effect in detail was beyond the scope of this paper, and we have not attempted a diameter correction for the magnitudes. Throughout the paper extinction-corrected magnitudes mean a correction for magnitudes only, unless noted otherwise. On the other hand, the colours given refer to a fixed aperture where a diameter correction is unnecessary for all galaxies larger than the aperture.

6. The catalogue

Table 2, which is available online at A&A, lists all the galaxies and galaxy candidates in the searched area. The columns are as follows.

Column 1: identity consisting of the lettering DZOA (for DENIS-ZOA) followed by the DENIS slot number and a consecutive number for each initial candidate.

Column 2: total number of sightings of same galaxy (e.g., on overlap regions or repeat observations). A plus denotes an additional observation from the pre-survey (these observations were used for verification only).

Column 3: Right Ascension and Declination (J2000). A colon after the coordinates indicates a lower positional accuracy (cf. Table 1). They were determined from the DSS-red images.

Column 4: Galactic longitude l and latitude b in degrees.

Column 5: B-band extinction A_B as derived from the reddening values $E(B-V)$ of the IRAS/DIRBE maps (Schlegel et al. 1998) using $A_B = 4.14\,E(B-V)$. Note that the extinction values are not calibrated for $|b| < 5°$ and may be unreliable. For the subsequent analysis, the extinctions in the NIR bands were calculated using Eqs. (1) in Sect. 3.

Column 6: classification of the candidate: *DG* stands for DENIS galaxy; *UG* stands for an uncertain galaxy; *BG* indicates a galaxy that was identified after consulting the WKK catalogue. *NG* stands for a B-band galaxy that was found to be non-galaxian with DENIS.

Column 7: visibility of the galaxy in the *B*-, *I*-, *J*-, and *K*-bands respectively, where 1 stands for a positive identification and 0 for a non-detection.

Column 8: morphological type of the galaxy as estimated from the appearance in all three NIR passbands as well as the DSS-red image. "E": elliptical galaxy; "S": spiral galaxy (with no possible differentiation between early- and late-type spiral); "SE": early-type spiral; "SM" medium-type spiral; "SL": late-type spiral (including irregulars). A question mark is given if a distinction between an elliptical galaxy and the bulge of a spiral galaxy was not possible. A dash is used where the object is not a galaxy (class *NG*).

Columns 9–11: total magnitudes and errors in *I*, *J*, and *K*, as derived using `SExtractor` (with the `MAG_AUTO` parameter). Note that a galaxy may be visible in one of the NIR bands but have no magnitudes depending on the ability of `SExtractor` to detect or deblend the object from its neighbours.

Columns 12–14: the colours and errors obtained from the 7″-aperture magnitudes as derived using `SExtractor` and corrected for reddening using the DIRBE/IRAS extinction values: $(I-J)^0$, $(I-K)^0$, and $(J-K)^0$.

Column 15: quality of the photometry for the *I*-band (first digit), *J*-band (second digit), and *K*-band (last digit): 0 means good photometry, 2 uncertainty in the 7″-aperture magnitude, 3 uncertainty in the total magnitude, and 4 uncertainty in both. 5 means the 7″-aperture magnitude is unreliable, 6 stands for unreliability in the total magnitude, and 7 means both are unreliable. A 9 indicates that the strip was non-photometric (strip 6052) and all photometry is unreliable (the estimated extinction due to the clouds in this case is $\sim 0\overset{\mathrm{m}}{.}25 - 0\overset{\mathrm{m}}{.}3$). Magnitudes with quality parameters 5–9 have been excluded in the further analysis.

Columns 16–18: the major diameters of the galaxies in *I*, *J*, and *K* in arcseconds, derived at an isophote of $21\overset{\mathrm{m}}{.}75$, $20\overset{\mathrm{m}}{.}5$, and $18\overset{\mathrm{m}}{.}0$, respectively. These isophotes have a comparable background noise in all three bands across the entire search area.

We discovered 83 galaxies (plus 38 uncertain candidates) on the 1073 searched images. 79 (33) of them are visible in the *I*-band, 82 (35) in *J*, and 67 (25) in *K*. Figure 3 shows the distribution of the detected galaxies: filled circles stand for definite galaxies, open circles show uncertain candidates. Crosses denote Galactic objects. The contours depict the extinctions at $A_B = 2^{\mathrm{m}}$, 3^{m}, 5^{m}, 10^{m}, 20^{m}, 30^{m}, 50^{m}, and 60^{m}, as indicated.

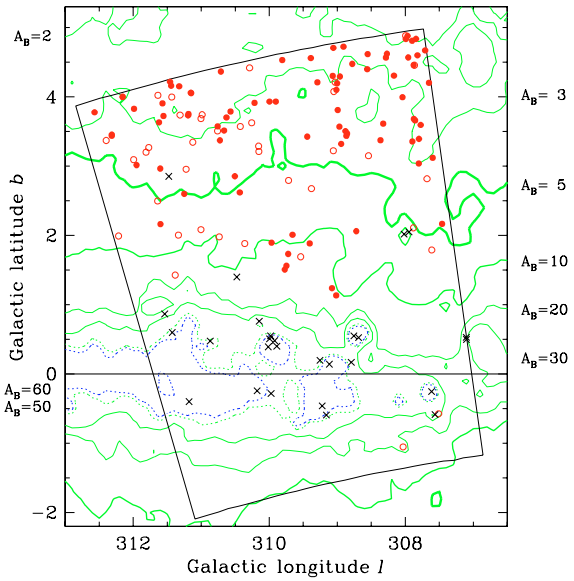

Fig. 3. Distribution of galaxies *(circles)* and Galactic objects *(crosses)* in the searched area (*tilted rectangle*). *Filled circles* are galaxies visible with DENIS, and *open circles* stand for uncertain galaxies. Extinction contours according to the IRAS/DIRBE maps are displayed as labelled. The galaxy PKS 1343 – 601 ($l = 309\overset{\circ}{.}7$, $b = +1\overset{\circ}{.}8$, $A_B = 12\overset{\mathrm{m}}{.}3$) is located close to the centre.

6.1. Notes on individual objects

In this section we describe some particularly interesting galaxies. Thumbnail images of these galaxies are presented in Fig. 4 with the *I*-, *J*-, and *K*-band image from left to right. The name of the galaxy is printed at the top and the *B*-band extinction and Galactic coordinates at the bottom. The *J*- and *K*-band images have been smoothed, and the cut values have been calculated separately for each image in dependence of the background.

DZOA4641-06 and **DZOA4645-13**: both these objects, classified as uncertain galaxies, have very high extinctions ($A_B = 39^{\mathrm{m}}$ and 24^{m}, respectively). They are only visible in the *K*-band and could be Galactic nebulae (e.g., H II regions). However, Galactic objects generally also have very red stars in the immediate surroundings (cf. images in Appendix B), which is not the case here. Moreover, an intrinsically bright galaxy at the cluster distance would indeed still be visible in the *K*-band: the extinction-corrected magnitudes are $K^0 = 8\overset{\mathrm{m}}{.}8$ and $8\overset{\mathrm{m}}{.}3$, respectively. For comparison, the central elliptical galaxy is only slightly brighter at $K^0 = 8\overset{\mathrm{m}}{.}0$, which would mean that these two galaxy candidates could lie at the distance of the cluster or closer.
The image of DZOA4645-13 indicates that it may even consist of a pair of galaxies; note, however, that the photometry refers to a single object.

DZOA4652-04/PKS 1343 – 601: the giant elliptical galaxy in the centre of the search area has an extinction corrected *K*-band magnitude of $8\overset{\mathrm{m}}{.}0$ and is the brightest galaxy (after extinction correction) in the whole search area. Since this galaxy is not visible on the ESO/SERC *B*-band plates we have derived an extinction-free *B*-band magnitude of $\sim 11\overset{\mathrm{m}}{.}8$ using $(B-K)^0 = 3\overset{\mathrm{m}}{.}83$ (Girardi et al. 2003) for elliptical galaxies.
Tashiro et al. (1998) present ASCA observations of the galaxy and its surroundings. They have also observed PKS 1343 – 601 with XMM. Both observations show a point-like emission from the galaxy centre, indicating it to have an active nucleus. A faint jet to the south-east in the direction of the radio lobes is clearly visible on the XMM and Chandra images. There is also faint diffuse emission connected with the galaxy. This is interpreted by Tashiro et al. as emission due to inverse Compton scattering in the radio lobes. It remains uncertain, whether part of the diffuse X-ray emission could actually be due to hot galaxy cluster gas. This will be discussed more deeply in Paper II.
To determine an X-ray flux for the galaxy, we used the XMM data from the three cameras (37 ks). We fitted a power law modified by absorption to the spectrum (it shows a negligible Fe line), and find a photon index of 1.58 ± 0.02, and a hydrogen column density of $N_{\mathrm{H}} = (1.65 \pm 0.03) \times 10^{22}$ cm^{-2}. We derive an unabsorbed X-ray flux [1–10 keV] of 7.66×10^{-12} erg cm^{-2} s^{-1} with a reduced χ^2 of 1.0. This leads to an integrated bolometric luminosity of $4.1 \times 10^{42}\ h_{70}^{-2}$ erg s^{-1}. The latter is suggestive of a weak AGN (cf. DZOA4653-11 below). Adopting the

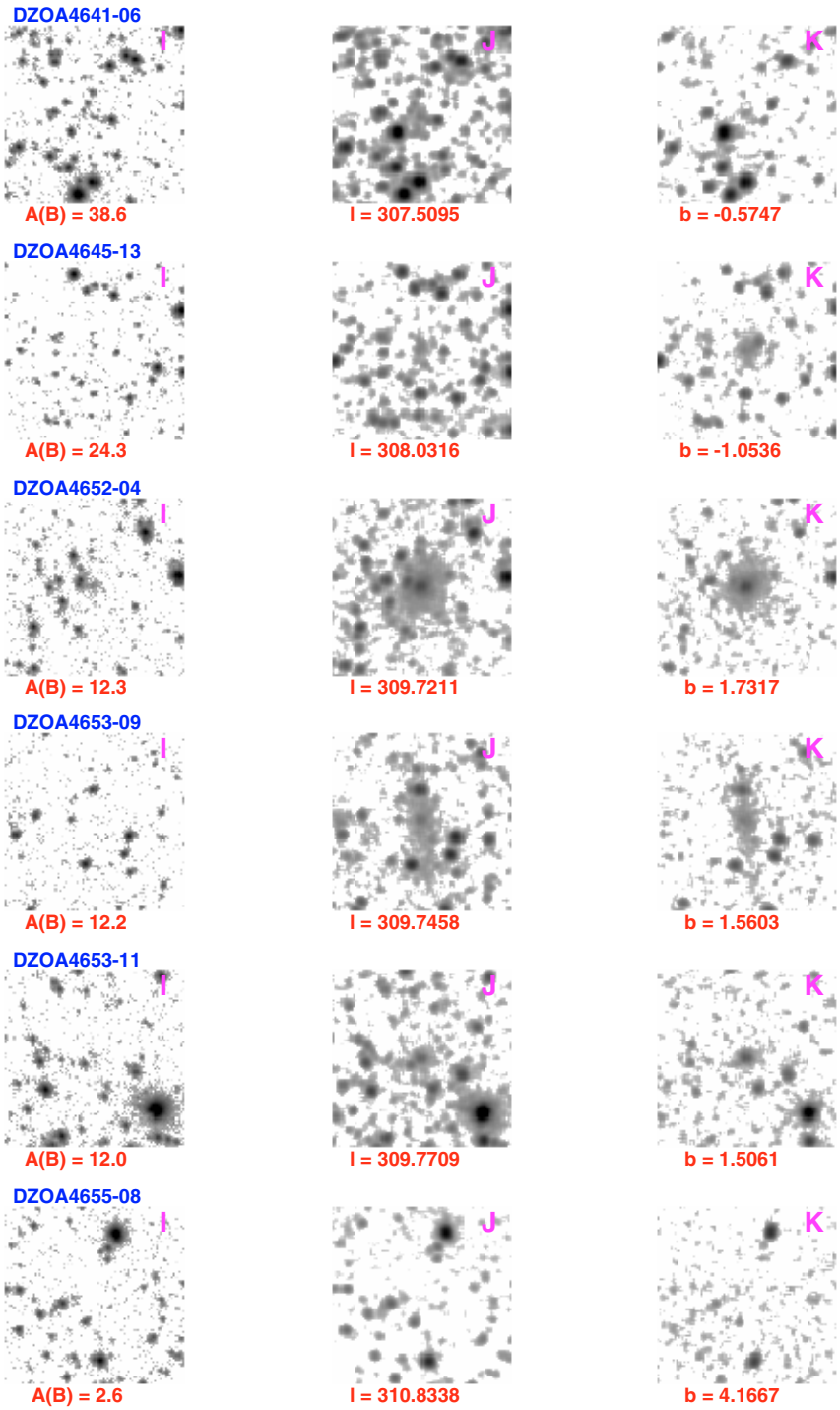

Fig. 4. *I*-, *J*-, and *K*-band images (*left, middle, and right hand column*, respectively) of the galaxies discussed in Sect. 6.1; the names are given at the top, *B*-band extinctions and Galactic coordinates at the bottom of the respective row of images of the galaxy. The minimum and maximum cut values for the *I*-band are 1.0 and 300, respectively, for the *J*-band they are 0.05 and 70, respectively, and for the *K*-band they are 0.1 and 70, respectively.

above derived *B*-band magnitude we find $\log L_B/L_\odot = 11.0$ and $\log L_X/L_B = 31.6$. Note that this value depends on the adopted $(B-K)$ colour (a change of $0\overset{m}{.}1$ leads to a change of 0.1 in $\log L_B/L_\odot$).

DZOA4653-09: this is the second largest galaxy within the cluster centre area. With an extinction corrected *K*-band magnitude of $9\overset{m}{.}1$ it is about 1^m fainter than PKS 1343 – 601. The extinction for both galaxies is very similar, but while PKS 1343 – 601 is visible in all passbands, DZOA4645-13 is only visible in the *J*- and *K*-bands. This suggests a lower surface brightness than for elliptical galaxies. DZOA4653-09 is therefore more likely to be an early or medium type spiral: in the *K*-band the bulge is quite distinct and shows an elongated faint halo.
This galaxy was not detected in the blind H I Parkes Multibeam survey of the ZoA (Schröder et al. 2005; Henning et al. 2005); it is therefore unlikely to be an H I-rich spiral at the cluster distance. On the other hand, being close

to the centre of the suspected cluster, this galaxy may be H I-deficient.

DZOA4653-11: this galaxy was discovered in the Galactic Plane optical identification programme of XMM-Newton serendipitous sources carried out by the Survey Science Centre (Motch et al. 2003; Watson et al. 2001). It was identified as a highly obscured AGN by Michel et al. (2004) though a significant part of the extinction is Galactic. It also has an entry in the serendipitous 1XMM catalogue (XMM-Newton Survey Science Centre 2003).
A deep *I*-band image obtained for the optical identification programme shows a bright bulge and very faint halo, which implies an early type spiral galaxy (see Fig. 1 in Piconcelli et al. 2006). The optical spectrum shows a prominent Hα line. Together with the [N II] lines ($\lambda\lambda$ 6548, 6583) and [S II] line (λ6731) this provides a heliocentric velocity of $v = 3628 \pm 12$ km s^{-1}, putting DZOA4653-09 right at the cluster distance (see also the velocity determinations in Schröder et al. 2005; Masetti et al. 2006; and Piconcelli et al. 2006).
The XMM-Newton spectrum is highly absorbed due to both intrinsic as well as Galactic absorption: using as a simple model a power law modified by absorption and a faint iron line (44 eV equivalent width), we found a photon index of 1.20 ± 0.02 and a hydrogen column density of $N_{\rm H} = (2.02 \pm 0.04) \times 10^{22}$ cm^{-2}. The Galactic column density at this point is only $N_{\rm H} = 1.07 \times 10^{22}$ cm^{-2}, hence there is significant intrinsic absorption (cf. PKS 1343 – 601).
Piconcelli et al. (2006) discuss this galaxy in more detail. They conclude that DZOA4653-09 is likely to be an intermediate Seyfert. Their more complex model gives an absorbed X-ray flux [1–10 keV] of 3.72×10^{-11} erg cm^{-2} s^{-1} with a reduced χ^2 of 0.94. According to Elvis et al. (1994) the intrinsic hard band luminosity (L_{2-10}) is about 3% of the bolometric luminosity for quasars, but Gandhi & Fabian (2003) find a value closer to 10% for Seyferts. Using the latter we derive a bolometric luminosity of $1.5 \times 10^{44}\ h_{70}^{-2}$ erg s^{-1}. We estimate the *B*-band magnitude to be $13\overset{\rm m}{.}0$ using the extinction-corrected *K*-band magnitude of $9\overset{\rm m}{.}48$ and the colour $(B-K)^0 = 3\overset{\rm m}{.}50$ (Girardi et al. 2003) for early-type spiral galaxies which is corrected for Galactic extinction as well as internal absorption (we assume the internal absorption to be negligible in the *K*-band). We find $\log L_B/L_\odot = 10.5$ and $\log L_X/L_B = 33.7$, a typical value for AGNs.

DZOA4655-08: this galaxy is the only one in the entire search area that was found in the *B*-band but is *not* visible on the DENIS images. For completeness reasons we have included it in our catalogue. DZOA4655-08 is a late type spiral and lies at a low extinction of $A_B = 2\overset{\rm m}{.}5$. This is consistent with the predictions in Fig. 1 to find more galaxies in the optical than in the NIR at low extinctions levels ($A_B < 2\overset{\rm m}{.}2$; note this limit depends quite strongly on morphological type and surface brightness).

6.2. Galactic objects

Separating Galactic objects from galaxies at high extinction levels can be confusing: Galactic nebulae, like galaxies, can be bright at longer wavelengths, either because of the large extinction or because of their intrinsically very red colours (e.g., young stellar objects). Most of them are found at very low latitudes and very high extinctions ($A_B > 50^{\rm m}$) and because of this are unlikely to be galaxies, but some were found at lower extinctions. We used similarities in form and colour in comparison with other Galactic objects and definite galaxies to classify cases at medium extinctions. In addition, a couple of Planetary Nebulae were found at low extinctions. These can be usually recognised by their sharp and sometimes irregular edges.

We have listed all objects believed to be Galactic in Table 3, and thumbnail images of them are shown in Appendix B of the A&A online version. Columns 1–7 are as described in Table 2. The coordinates are either the estimated centre of the nebulosity or indicate the most prominent feature connected with it. Note that the extinctions given in Col. 5 are total extinctions along the line-of-sight through our Galaxy, i.e., the actual extinction for a Galactic object can be anywhere between zero and the total extinction. Where possible, the classification in Col. 6 indicates Planetary Nebulae (PN), reflection nebulae (RN), H II regions, and young stellar objects (YSO) which show one or several very red stars and some diffuse emission connected with it. The visibility in the *B*-band in Col. 7 refers to the SSS[3]-blue images. Column 8 gives the name in the literature as found with NED[4]: 2MASX stands for the 2MASS[5] all-sky extended source catalogue (Two Micron All Sky Survey team), PMN for Parkes-MIT-NRAO Radio Survey (Griffith et al. 1994), AM for Arp & Madore (1987), and KK for Karachentseva & Karachentsev (2000).

7. Comparison with other catalogues

We have searched NED for known galaxies in our search area. Apart from 2MASS and WKK counterparts only few others had been observed before, most of them in the radio. They are all listed in Table 4. For quick reference we repeat the DENIS-ID (Col. 1), coordinates (Col. 2), extinction (Col. 3), class (Col. 4), and visibility (Col. 5) from the Cols. 1, 3, 5–7 in Table 2, respectively. Column 6 gives the 2MASS-ID from the extended source catalogue (Two Micron All Sky Survey team 2003); Col. 7 gives the WKK name and the last column gives other IDs from other catalogues. These are IRAS for the IRAS Point Source Catalog (IRAS PSC; Joint IRAS Science Working Group 1988), PMN for Parkes-MIT-NRAO Radio Survey (Griffith et al. 1994), HIZOA for Juraszek et al. (2000), HIZSS for the H I Parkes ZoA Shallow Survey (Henning et al. 2000), NW04 for Nagayama et al. (2004), PKS for the Parkes Catalog of radio sources (Wright & Otrupcek 1990) 4U for the Fourth Uhuru Catalog of X-ray Sources (Forman et al. 1978), and 1XMM for the First XMM-Newton Serendipitous Source Catalogue (XMM-Newton Survey Science Centre 2003).

7.1. B-band

The WKK catalogue lists 35 galaxies within our search area. One galaxy (WKK2589, DZOA4655-08) is not visible on the DENIS images. It is a small, very low surface brightness galaxy, probably Sm or Irr. Five *B*-band galaxies, all classified as uncertain galaxies by WKK, were identified as (blended) stars with the higher spatial resolution of the DENIS *I*-band images (they are classified as *NG* in Table 2). Figure 5 shows the WKK galaxies as plus signs overlaid over the plot shown in Fig. 3.

As expected from Fig. 1, most *B*-band galaxies are found in the low extinction regions. The highest extinction for a *B*-band galaxy in the searched area is $A_B = 5\overset{\rm m}{.}2$ (DZOA4641-07,

[3] The SuperCOSMOS Sky Survey (Hambly et al. 2001).
[4] the NASA/IPAC Extragalactic Database.
[5] see `http://irsa.ipac.caltech.edu/Missions/2mass.html`

Table 3. Galactic objects detected in the search area.

Ident.	N	RA (J2000)	Dec	Gal ℓ	Gal b	$A_B^{\rm tot}$	Class	Visibil.	Other name
(1)	(2)	(3a)	(3b)	(4a)	(4b)	(5)	(6)	(7)	(8)
DZOA4638-16	1	13 27 08.5	–62 03 17	307.10	0.53	28.9	...	0 0 0 1	2MASXJ13270813-6203201
DZOA4638-13	2	13 27 10.4	–62 05 05	307.10	0.50	28.1	...	0 0 1 1	
DZOA4641-10[a]	2	13 32 12.4	–60 25 33	307.94	2.05	12.5	...	1 1 1 1	
DZOA4641-12	5	13 32 30.9	–62 45 06	307.61	–0.25	127.6	HII?	0 1 1 1	
DZOA4642-09	6	13 32 31.4	–63 05 22	307.56	–0.59	50.0	HII	0 0 1 1	PMNJ1332-6305
DZOA4642-07	3	13 32 48.8	–60 26 44	308.02	2.02	21.0	YSO	1 1 1 1	2MASXJ13324576-6026565, AM1326-601
DZOA4647-04	1	13 40 26.4	–61 47 57	308.69	0.52	100.8	YSO	0 0 0 1	
DZOA4648-07	1	13 40 57.6	–61 45 44	308.75	0.55	113.4	...	0 0 1 1	2MASXJ13405761-6145447
DZOA4649-10	3+	13 41 54.8	–62 07 43	308.79	0.17	39.9	...	0 1 1 1	
DZOA4650-12	4++	13 44 39.3	–62 05 31	309.12	0.14	94.2	HII	0 0 0 1	
DZOA4651-13	1	13 45 42.4	–62 00 32	309.25	0.20	46.0	...	0 0 0 1	
DZOA4652-10[b]	1	13 46 20.8:	–62 48 02:	309.16	–0.59	57.2	...	0 1 1 1	2MASXJ13462058-6247597
DZOA4652-09	1	13 46 37.4:	–62 39 27:	309.22	–0.46	111.9	HII?	0 0 1 1	2MASXJ13463702-6239303
DZOA4655-12	1	13 50 35.4	–61 40 18	309.89	0.40	143.4	YSO	0 0 1 1	2MASXJ13503488-6140199, (PMNJ1350-6141)
DZOA4655-11	2	13 50 41.8	–61 35 09	309.92	0.48	151.6	YSO	0 0 0 1	
DZOA4655-09[c]	1	13 51 02.6	–61 30 15	309.98	0.55	77.0	...	0 0 1 1	2MASXJ13510266-6130150
DZOA4655-10	2	13 51 14.7	–61 32 35	309.99	0.51	97.5	...	0 0 1 1	
DZOA4656-08[d]	1	13 51 37.9	–61 39 07	310.01	0.39	113.2	...	0 1 1 1	
DZOA4656-06	1	13 51 59.8	–61 15 41	310.15	0.76	60.5	HII?	0 0 0 1	2MASXJ13515956-6115394
DZOA4657-05	2	13 52 37.3	–62 19 00	309.97	–0.28	55.8	...	0 0 1 1	
DZOA4657-06	2	13 53 23.3	–60 33 48	310.48	1.40	11.2	PN	1 1 1 1	
DZOA4658-07	1	13 54 15.9:	–62 13 46:	310.18	–0.24	76.5	RN	1 1 1 1	KK2000-60
DZOA4661-02	2	13 58 13.8	–58 54 31	311.48	2.85	4.4	PN	1 1 1 1	
DZOA4661-05	1	13 58 23.9	–61 21 45	310.87	0.47	57.1	...	0 0 0 1	
DZOA4664-05	2	14 02 36.2	–61 05 44	311.43	0.60	57.2	HII?	0 0 1 1	2MASXJ14023620-6105450
DZOA4664-04	1	14 02 52.9	–60 48 27	311.54	0.86	29.0	...	0 0 1 1	
DZOA4664-06	1	14 02 52.9	–62 07 22	311.18	–0.40	93.6	HII?	0 0 0 1	

[a] While this object shows two apparent point sources in the K-band, the B- and I-bands clearly show an elongated compact extended emission with the brightest part positioned on one of the point sources.
[b] This object shows diffuse emission, as well as clumps, and possibly a dust lane. It could be a PN or a YSO seen on-edge.
[c] Very faint, it seems to show comparable features to DZOA4652-10 and DZOA4656-08.
[d] An extremely bright point source in the K-band, is also shows diffuse and clumpy extended emission and possible a dust lane in all bands.

WKK2301). The completeness limit for $B^0 = 15\overset{\rm m}{.}5$ and $D^0 = 60''$ of the WKK-catalogue is $A_B = 3^{\rm m}$ (Woudt & Kraan-Korteweg 2001).

The B-band magnitudes are isophotal and comparable to the B_{25} magnitudes. To derive (Galactic) extinction-corrected colours $(B-I)^0$, $(B-J)^0$, and $(B-K)^0$ for our galaxies we have therefore used the total I-, J-, and K-band Kron-magnitudes. Note that these are more uncertain than colours from a fixed aperture due to problems with star subtraction. In addition, at high extinctions it is necessary to correct the diameters as well as the magnitudes (Cameron 1990). However, the diameter correction for NIR data has not been investigated to date (cf. Sect. 5); hence, we have only applied a magnitude correction. Since the diameter correction affects mainly the disk we have not attempted to derive colours for the SL-types.

The mean corrected colours, the standard deviation, and the number of galaxies are given in Table 5 along with respective values taken from Girardi et al. (2003; field and group galaxies) and from Moriondo et al. (2001; galaxies in the Pisces-Perseus cluster), where the latter two are corrected both for Galactic extinction as well as for internal absorption. Since Moriondo et al. give only NIR photometry we have extracted the two correction terms as well as the corrected B- and I-band data from the LEDA[6] database. Both samples agree very well for $(B-K)$, despite the large difference in the number of galaxies.

[6] the Lyon-Meudon Extragalactic DAtabase, see `http://leda.univ-lyon1.fr`.

We have not attempted to correct our data for internal absorption since the inclinations, as well as the morphological classifications, are uncertain at these high foreground extinction levels. We therefore turned this correction off for the Moriondo et al. sample (see last entry in Table 5) to better compare it with our sample. The colours agree reasonably well within the errors, except for the sample of elliptical galaxies where only a couple of galaxies contribute to the mean value: the standard deviation for the two ellipticals in our sample is very small and they are clearly not representative.

The colours of our SM-sample are nominally redder than the colours of our SE-sample. On the other hand, the standard deviations of the two subsamples are at least twice as large as the ones for the Moriondo et al. samples. Obviously, this effect is partly due to the large uncertainties in morphological types of our sample. In addition, while for large samples the statistical mean is little affected by the (unknown) individual inclination-dependent corrections, small samples may be highly biased, and the statistical means as well as the scatter may vary widely solely due to a different distribution in inclinations.

Consequently, we can only say that the colours of these two (small) subsamples appear to be similar. For example, if we include the colours of one galaxy found south of our search area (WKK2503 at $l = 308\overset{\circ}{.}41$ and $b = -3\overset{\circ}{.}38$) to the SM-sample, we find $(B-I)^0 = 1.43$ instead of 1.70, $(B-J)^0 = 2.53$ instead of 2.82, and $(B-K)^0 = 3.59$ instead of 3.93, which agrees much better with the Moriondo et al. colours.

Table 4. Cross-identifications with other catalogues.

Ident.	RA (J2000)	Dec	A_B	Class	Visibil.	2MASX	WKK	Other names
(1)	(2a)	(2b)	(3)	(4)	(5)	(6)	(7)	(8)
DZOA4638-04	13 27 20.3	–57 52 08	2.8	*DG*	0 1 1 1	J13272018-5752081		
DZOA4638-09	13 27 25.1	–58 20 28	2.6	*DG*	0 1 1 1	J13272507-5820282		
DZOA4638-03	13 28 10.0	–57 41 09	3.0	*DG*	0 1 1 1	J13280986-5741102		
DZOA4638-11	13 28 10.3	–60 22 59	5.0	*DG*	0 1 1 1	J13281021-6022580		
DZOA4638-10	13 28 11.0	–59 25 09	3.1	*DG*	0 1 1 0			
DZOA4638-06	13 28 15.4	–57 55 21	2.7	*DG*	0 1 1 1			
DZOA4638-01	13 28 37.1	–57 42 19	2.9	*DG*	1 1 1 1	J13283697-5742188	WKK 2267	
DZOA4639-07	13 28 44.4	–58 03 32	2.8	*UG*	0 1 1 0			
DZOA4639-06	13 28 49.7	–58 03 21	2.7	*DG*	1 1 1 1	J13284958-5803228	WKK 2271	
DZOA4639-19	13 29 00.3	–58 55 30	2.6	*BG*	1 1 1 0		WKK 2274	
DZOA4639-02	13 29 01.7	–57 37 32	3.0	*DG*	0 1 1 0			
DZOA4639-14	13 29 10.4	–59 42 27	4.1	*UG*	0 1 1 0			
DZOA4639-01	13 29 14.7	–57 37 06	3.1	*UG*	0 1 1 1			
DZOA4639-03	13 29 16.1	–57 39 56	2.9	*DG*	0 1 1 1	J13291609-5739562		
DZOA4639-05	13 29 17.7	–57 56 03	2.7	*DG*	1 1 1 1	J13291753-5756032	WKK 2278	
DZOA4639-10	13 29 25.8	–59 07 11	2.6	*DG*	0 1 1 1			
DZOA4639-09	13 29 33.2	–58 50 54	3.0	*DG*	1 1 1 1	J13293316-5850552	WKK 2281	
DZOA4639-08	13 29 40.9	–58 49 30	3.1	*DG*	0 1 1 1			
DZOA4639-16	13 29 50.5	–60 44 05	5.8	*UG*	0 1 1 1			
DZOA4639-13	13 29 51.9	–59 28 19	3.1	*DG*	1 1 1 1		WKK 2285	
DZOA4640-05	13 30 13.4	–59 08 34	3.1	*DG*	0 1 1 1			
DZOA4640-03	13 30 34.6	–58 29 24	3.4	*DG*	1 1 1 1	J13303446-5829247	WKK 2292	
DZOA4640-02	13 31 09.6	–58 09 45	2.8	*DG*	0 1 1 1	J13310962-5809453		
DZOA4641-01	13 31 33.3	–57 50 04	2.7	*DG*	1 1 1 1	J13313318-5750054	WKK 2300	
DZOA4641-04	13 31 36.6	–60 22 37	5.8	*UG*	0 0 1 1			
DZOA4641-02	13 31 43.7	–57 53 11	2.8	*DG*	1 1 1 1	J13314368-5753125	WKK 2303	
DZOA4641-06	13 32 03.3	–63 05 06	38.5	*UG*	0 0 0 1			
DZOA4642-04	13 33 11.8	–58 49 22	4.0	*DG*	1 1 1 1		WKK 2327	
DZOA4642-01	13 33 39.2	–57 47 42	2.8	*DG*	1 1 1 1	J13333914-5747422	WKK 2334	
DZOA4642-06	13 33 47.6	–59 03 07	3.9	*DG*	1 1 1 1		WKK 2336	
DZOA4642-02	13 33 58.2	–58 00 29	3.2	*DG*	1 1 1 1		WKK 2338	
DZOA4644-04	13 35 26.0	–59 14 38	4.1	*UG*	0 1 1 1			
DZOA4644-02	13 35 30.1	–57 53 47	3.4	*DG*	0 1 1 0			
DZOA4644-01	13 36 08.1	–57 37 48	2.7	*DG*	0 1 1 1			
DZOA4645-01	13 37 05.0	–58 02 40	3.1	*DG*	0 1 1 1			
DZOA4645-14	13 37 15.2	–57 37 11	2.7	*BG*	1 1 1 0		WKK 2386	
DZOA4645-13	13 37 20.7	–63 28 12	24.3	*UG*	0 0 1 1			
DZOA4645-09	13 37 24.7	–58 52 21	4.5	*DG*	1 1 1 1	J13372458-5852216	WKK 2390	
DZOA4645-04	13 37 31.9	–58 08 01	3.1	*DG*	0 1 1 1			
DZOA4645-08	13 37 32.8	–58 50 04	4.5	*DG*	1 1 1 1	J13373272-5850056	WKK 2392	
DZOA4645-10	13 37 32.9	–58 54 14	4.5	*DG*	0 1 1 1	J13373282-5854136		IRAS 13342-5830 PMN J1337-5854
DZOA4645-03	13 37 44.1	–58 06 37	3.0	*UG*	0 1 1 1			
DZOA4645-05	13 37 44.3	–58 13 26	3.5	*DG*	1 1 1 0		WKK 2397	
DZOA4645-02	13 37 51.3	–58 00 59	2.9	*DG*	0 1 1 0			
DZOA4645-07	13 37 59.2	–58 30 55	4.7	*DG*	0 1 1 1	J13375912-5830556		
DZOA4646-01	13 38 03.3	–58 14 27	3.5	*UG*	0 1 1 1			
DZOA4646-03	13 38 08.5	–58 45 19	4.1	*DG*	0 1 1 1	J13380855-5845197		
DZOA4646-04	13 38 16.6	–59 00 15	4.3	*DG*	0 1 1 1			
DZOA4646-06	13 38 21.7	–60 17 02	9.0	*DG*	0 1 1 1			
DZOA4647-03	13 39 17.6	–59 04 46	4.3	*UG*	0 1 1 1			
DZOA4647-01	13 39 39.7	–58 04 00	3.5	*DG*	0 1 1 1	J13393970-5804007		
DZOA4647-02	13 39 52.7	–57 42 17	2.6	*DG*	1 1 1 1		WKK 2435	
DZOA4649-02	13 41 54.8	–58 48 28	3.9	*DG*	0 1 1 1			IRAS 13386-5832 HIZOA J1341-58
DZOA4649-07	13 42 09.8	–61 08 18	12.0	*DG*	0 0 1 1			
DZOA4649-06	13 42 29.6	–61 01 23	13.0	*DG*	0 0 1 1			HIZSS 082 HIZOA J1342-61
DZOA4649-03	13 42 35.6	–59 33 18	6.7	*UG*	0 1 1 0			
DZOA4649-01	13 42 59.9	–57 39 06	2.5	*DG*	1 1 1 1		WKK 2483	
DZOA4650-09	13 44 03.7	–60 19 35	10.4	*DG*	0 1 1 1	J13440358-6019350		
DZOA4650-01	13 44 36.5	–58 13 10	3.9	*DG*	0 1 1 1			
DZOA4651-05	13 45 00.2	–59 22 17	6.2	*UG*	0 1 1 0			
DZOA4651-02	13 45 17.7	–58 12 01	3.5	*DG*	0 1 1 0			
DZOA4651-08	13 45 25.3	–60 29 14	11.9	*UG*	0 0 1 1			NW04-03
DZOA4651-06	13 45 50.7	–60 09 05	8.2	*DG*	0 1 1 1	J13455154-6009067		NW04-08
DZOA4652-01	13 46 40.3:	–57 39 50:	2.3	*UG*	0 1 1 1			

Table 4. continued.

Ident.	RA (J2000)	Dec	A_B	Class	Visibil.	2MASX	WKK	Other names
(1)	(2a)	(2b)	(3)	(4)	(5)	(6)	(7)	(8)
DZOA4652-04	13 46 48.9:	–60 24 29:	12.3	*DG*	0 1 1 1	J13464910-6024299		NW04-24 PKS 1343-601 Centaurus B
DZOA4652-02	13 46 57.3:	–58 10 19:	3.3	*DG*	0 1 1 0			HIZOA J1347-58
DZOA4653-09	13 47 18.5	–60 34 13	12.2	*DG*	0 0 1 1	J13471848-6034133		NW04-38
DZOA4653-03	13 47 32.3	–58 47 45	3.8	*UG*	0 1 1 0			
DZOA4653-11	13 47 36.2	–60 37 04	12.0	*DG*	0 1 1 1			NW04-45 4U 1344-60 1XMM J134736.1-603704
DZOA4653-04	13 47 38.2	–58 52 15	4.3	*UG*	0 1 1 0			
DZOA4653-01	13 47 44.1	–58 26 38	3.8	*UG*	0 1 1 1			
DZOA4653-07	13 48 27.5	–60 11 47	10.7	*DG*	0 1 1 1			NW04-51
DZOA4654-03	13 49 04.0	–58 27 34	3.2	*UG*	0 1 1 1			
DZOA4654-04	13 49 41.3	–57 48 40	2.6	*NG*	1 1 0 0		WKK 2559	
DZOA4654-02	13 49 46.1	–58 13 04	2.6	*DG*	1 1 1 1	J13494605-5813040	WKK 2562	
DZOA4654-01	13 49 49.9	–57 37 25	2.5	*DG*	1 1 1 0		WKK 2564	
DZOA4655-01	13 50 21.3	–58 17 12	2.9	*DG*	0 1 1 1	J13502126-5817121		
DZOA4655-04	13 50 47.0	–59 23 08	6.0	*DG*	0 1 1 1	J13504691-5923083		
DZOA4655-07	13 50 51.8	–57 43 02	2.6	*NG*	1 1 1 0		WKK 2586	
DZOA4655-03	13 50 55.3	–59 08 29	4.1	*DG*	0 1 1 1			
DZOA4655-02	13 50 56.5	–58 27 46	3.5	*DG*	0 1 1 1			
DZOA4655-08	13 51 03.5	–57 47 15	2.6	*BG*	1 0 0 0		WKK 2589	
DZOA4656-01	13 51 31.9	–58 23 01	3.0	*DG*	0 1 1 1			
DZOA4656-04	13 51 33.9	–60 07 17	9.2	*UG*	0 1 1 1			
DZOA4656-03	13 51 38.6	–58 35 15	4.1	*DG*	1 1 1 1	J13513848-5835153	WKK 2596	IRAS 13483-5820 HIZSS 084 HIZOA J1351-58
DZOA4656-02	13 51 39.8	–58 26 48	3.2	*UG*	0 1 0 0			
DZOA4657-03	13 52 55.4	–58 09 59	2.3	*UG*	0 1 1 1			
DZOA4657-04	13 53 08.7	–58 12 59	2.4	*UG*	0 1 1 0			
DZOA4657-02	13 53 32.4	–57 49 30	2.7	*DG*	0 1 1 1			
DZOA4657-01	13 53 34.1	–57 49 10	2.7	*DG*	0 1 1 1	J13533399-5749098		
DZOA4658-06	13 54 18.1:	–59 56 14:	10.1	*UG*	0 1 1 0			
DZOA4658-04	13 54 23.1:	–58 06 30:	2.5	*DG*	0 1 1 1	J13542319-5806299		
DZOA4658-03	13 54 27.3:	–58 07 35:	2.6	*DG*	1 1 1 1	J13542749-5807328	WKK 2660	
DZOA4658-01	13 54 38.5:	–57 41 11:	2.3	*DG*	1 1 1 0		WKK 2669	
DZOA4658-05	13 54 39.5:	–58 31 07:	3.4	*UG*	0 1 1 1			
DZOA4659-13	13 55 18.4	–58 05 32	2.8	*UG*	0 1 1 1			
DZOA4659-11	13 55 29.0	–57 38 59	2.4	*BG*	1 1 1 0		WKK 2684	
DZOA4659-10	13 55 29.5	–57 35 26	2.4	*BG*	1 1 1 0		WKK 2686	
DZOA4659-01	13 55 43.5	–57 48 38	2.9	*UG*	0 1 1 1	J13554342-5748384		
DZOA4659-02	13 56 07.7	–58 52 21	3.8	*UG*	0 1 1 1			
DZOA4659-05	13 56 09.7	–59 46 14	8.2	*UG*	0 1 1 1			
DZOA4660-06	13 56 42.9	–59 11 16	5.1	*NG*	1 1 1 1		WKK 2708	
DZOA4660-02	13 56 52.3	–57 51 53	2.5	*DG*	1 1 1 1		WKK 2714	
DZOA4660-05	13 57 01.5	–59 12 35	5.4	*DG*	0 1 1 1	J13570135-5912362		
DZOA4660-03	13 57 06.7	–58 02 43	2.9	*DG*	0 1 1 1			
DZOA4660-01	13 57 08.2	–57 44 09	2.6	*UG*	0 1 1 1			
DZOA4660-04	13 57 46.6	–58 07 01	3.0	*DG*	0 1 1 1	J13574653-5807028		
DZOA4661-04	13 58 40.7	–58 18 13	3.6	*NG*	1 1 1 0		WKK 2755	
DZOA4661-03	13 58 52.6	–59 45 47	8.9	*UG*	0 1 1 1			
DZOA4661-01	13 58 57.0	–58 46 02	4.3	*DG*	1 1 1 1	J13585694-5846014	WKK 2764	
DZOA4662-02	13 59 35.7:	–58 25 49:	4.5	*UG*	0 1 1 1	J13593587-5825489		
DZOA4662-03	14 00 01.9:	–58 29 06:	4.8	*UG*	0 1 1 0			
DZOA4662-01	14 00 04.0:	–57 50 02:	2.7	*DG*	1 1 1 1		WKK 2785	
DZOA4662-04	14 00 10.9:	–59 12 35:	5.3	*UG*	0 1 1 0			
DZOA4662-07	14 00 26.9:	–60 18 31:	15.4	*UG*	0 0 1 1			
DZOA4663-05	14 00 33.9	–59 32 32	6.6	*DG*	0 1 1 1			
DZOA4663-02	14 00 55.3	–57 37 23	2.9	*DG*	0 1 1 0			
DZOA4663-01	14 00 55.8	–57 37 28	2.9	*DG*	0 1 1 0	J14005571-5737279		
DZOA4663-04	14 01 25.6	–58 37 37	4.4	*DG*	0 1 1 1			
DZOA4663-03	14 01 35.4	–58 32 22	4.3	*UG*	0 1 1 0			
DZOA4664-03	14 02 42.0	–57 44 08	3.3	*NG*	1 1 0 0		WKK 2872	
DZOA4664-02	14 03 11.2	–58 06 20	3.6	*DG*	0 1 1 1	J14031094-5806201		
DZOA4665-02	14 03 13.8	–58 07 13	3.6	*DG*	0 1 1 1	J14031384-5807141		
DZOA4665-03	14 03 57.5	–58 09 49	4.0	*UG*	0 1 1 1			
DZOA4665-01	14 04 21.0	–57 43 33	2.9	*DG*	0 1 1 1	J14042102-5743339		
DZOA4666-01	14 05 35.9	–59 32 19	8.5	*UG*	0 1 1 1			

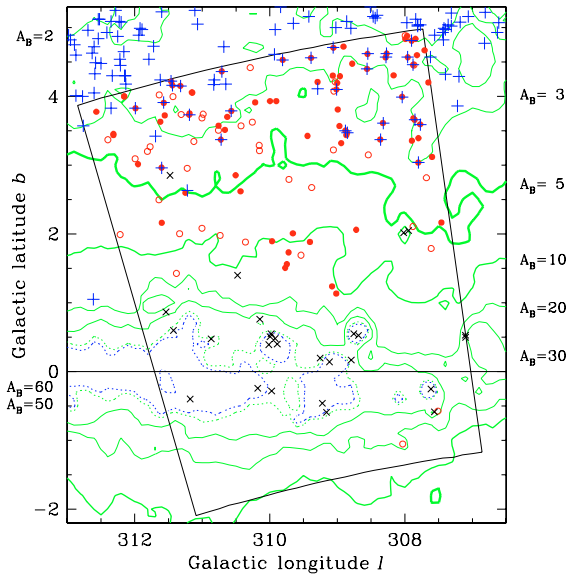

Fig. 5. Same as Fig. 3, but with *B*-band galaxies (*plus signs*) from Woudt & Kraan-Korteweg (2001) overlaid.

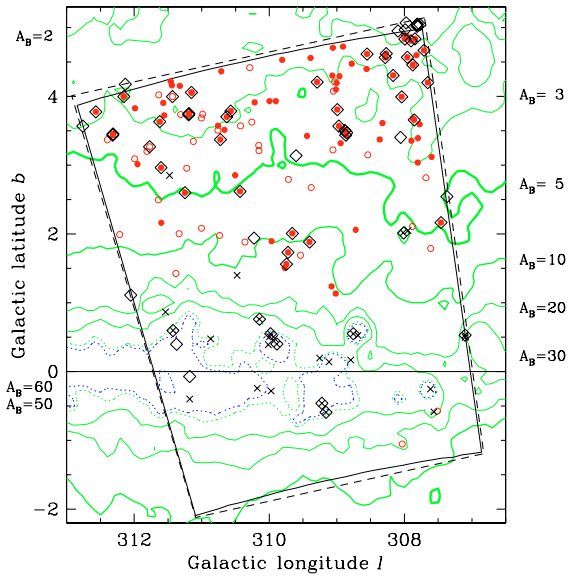

Fig. 6. Same as Fig. 3, but with 2MASS galaxies (*diamonds*) overlaid. The 2MASS extraction region is marked with a *dashed* rectangle.

Table 5. Comparisons of colours.

Type	$(B-I)^{0,\mathrm{corr}}$			$(B-J)^{0,\mathrm{corr}}$			$(B-K)^{0,\mathrm{corr}}$		
	mean	σ	n	mean	σ	n	mean	σ	n
This work (with Galactic extinction correction only):									
E	2.31	0.01	2	3.60	0.20	2	4.40	0.03	2
SE	1.70	0.74	7	2.63	0.93	7	3.53	1.21	6
SM	1.70	0.71	9	2.82	0.84	8	3.93	0.80	6
Girardi et al. 2003 (with full corrections):									
E+S0							3.83	0.03	145
S0+SE							3.79	0.03	157
SM							2.98	0.03	507
Moriondo et al. 2001 (with full corrections):									
E	2.40		1	2.86	0.47	3	3.80	0.46	3
SE	1.81	0.28	4	2.53	0.20	8	3.50	0.36	8
SM	1.41	0.38	15	2.23	0.32	17	3.07	0.34	17
Moriondo et al. 2001 (with Gal. extinction correction only):									
E	2.40		1	2.87	0.48	3	3.81	0.47	3
SE	2.06	0.33	4	2.81	0.29	8	3.81	0.34	8
SM	1.69	0.30	15	2.59	0.32	17	3.49	0.35	17

Furthermore, Monnier Ragaigne et al. (2003) quote $(B-K) = 4.0$ for a predominantly early-type sample and colours as blue as $(B-K) = 2.7$ for infrared low surface brightness galaxies (while they corrected the *B*-band data for Galactic extinction and internal absorption, the corrections for the *K*-band data were assumed to be negligible). These values denote the large range of $(B-K)$ colours that can be found for galaxies in general, which implies in turn that small subsamples are sensitive to any uncertainties in morphological types.

7.2. 2MASS J- and K-band comparison

We have extracted all objects from the 2MASS all-sky extended source catalogue (Two Micron All Sky Survey team 2003) within the region 13.45 < RA < 14.11 and −63.8 < Dec < −57.4. There are 65 objects, 11 of which are just outside the searched DENIS area. Figure 6 shows the distribution of the extended 2MASS objects together with their extraction region.

Forty-nine objects are common to both data sets, and five 2MASS objects were not found with DENIS. Of the 49 objects in common, 9 are classified by us as Galactic objects, and two as an uncertain galaxy. Of the five 2MASS objects that were not found in the DENIS search, visual inspection of DENIS images indicates that two are at very high extinctions: one is very probably a Galactic object, while the other seems to be a small star very close to a bright star (this can also be seen on the 2MASS *J*-band image). The third object is probably a faint double star with a very small spatial separation (it is slightly elongated but does not appear to be diffuse on the 2MASS images), while the last two are very small but bright galaxies that were not recognised as such in the DENIS search.

Of the 45 DENIS galaxies that were not in the 2MASS extended source catalogue most will be detected in the 2MASS point source catalogue, except for a few late type galaxies that are too faint in *J* and *K* and could only be found through the DENIS *I*-band.

This gives a rough estimate of the reliability of 80% for the automatic 2MASS extraction for galaxies in this highly confused and obscured region, while the completeness of the 2MASS galaxy extraction in this area is slightly less than 50%.

We compare the *J*- and *K*-band magnitudes of the 2MASS galaxies with our magnitudes in Fig. 7. The upper panel shows the differences in the *J*-band with a mean of $0\overset{\mathrm{m}}{.}10 \pm 0\overset{\mathrm{m}}{.}07$ and a standard deviation of $0\overset{\mathrm{m}}{.}42$. In the *K*-band (middle panel) the mean of the differences is $0\overset{\mathrm{m}}{.}31 \pm 0\overset{\mathrm{m}}{.}05$ with a standard deviation of $0\overset{\mathrm{m}}{.}32$, which indicates that there is a substantial offset between the two catalogues in the *K*-band. This offset can be explained by the large difference in magnitude limits of the two surveys: the 10σ sensitivity limit for extended sources with 2MASS are $13\overset{\mathrm{m}}{.}1$ and $13\overset{\mathrm{m}}{.}9$ for *K* and *J*, respectively (Jarrett et al. 2000a), while the much deeper 3σ extraction limit for extended sources with DENIS are only $12\overset{\mathrm{m}}{.}0$ and $14\overset{\mathrm{m}}{.}8$, respectively (Mamon 1998, 2000). Note, though, that these limits refer to high Galactic latitudes only. If we use the 2MASS isophotal *K*-band magnitudes (at 20^{m} per square arcsecond) instead, the mean of the differences is only $0\overset{\mathrm{m}}{.}19 \pm 0\overset{\mathrm{m}}{.}05$ with a standard deviation of $0\overset{\mathrm{m}}{.}31$ (bottom panel).

We find a similar difference between the 2MASS major diameter at the *K*-band 20^{m}-per-square-arcsecond isophote and the DENIS major diameter that we have derived with `ds9` at

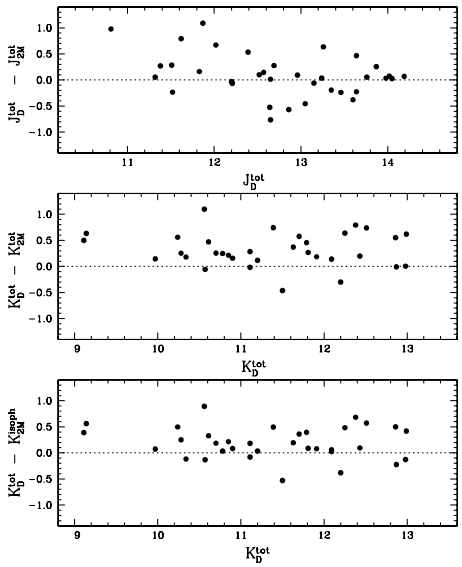

Fig. 7. The difference of total DENIS and 2MASS magnitudes is plotted versus DENIS total magnitudes in J (*upper panel*) and in K (*middle panel*); the difference between DENIS total and 2MASS isophotal K-band magnitudes is shown in the *bottom panel*.

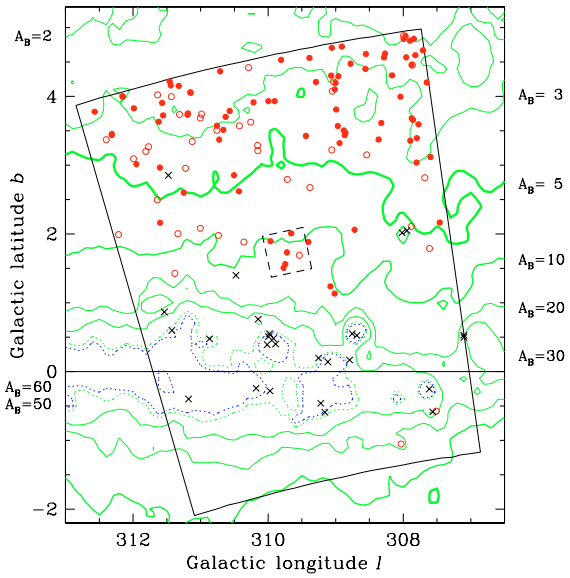

Fig. 8. Same as Fig. 3, but with the area searched by Nagayama et al. overlaid as a small (*dashed*) rectangle.

the K-band $18^{\rm m}$-per-square-arcsecond isophote in such a way that the 2MASS diameters are systematically larger, as expected given that their isophote is 2 mag fainter. Hence, the 2MASS total magnitudes are indeed expected to be brighter than those we derive. In particular, we find

$$\log D_{\rm D} - \log D_{\rm 2M} = (-0.73 \pm 0.03)\ \log D_{\rm D} + (0.12 \pm 0.03)$$

where the diameters are given in arcseconds. The rms difference is 0.04.

Using the 2MASS isophotal J-band the change in offset is negligible (the mean is now $0\overset{\rm m}{.}04 \pm 0\overset{\rm m}{.}07$ with $\sigma = 0\overset{\rm m}{.}34$; not shown) as expected by the smaller difference in limiting magnitudes. This means, that the DENIS J-band photometry is very close to the isophotal magnitude at $20^{\rm m}$ per square arcsecond.

7.3. K-band

Nagayama et al. (2004) have obtained deep K-band images of an area of $36' \times 36'$ around PKS 1343 – 601. Figure 8 shows this area as a dashed rectangle overlaid in Fig. 3. The plot does not show the detections by Nagayama et al. since the spatial density of these detections is very high due to the much deeper imaging. All six DENIS galaxies in this region (including one uncertain candidate) have been detected by them as well.

Comparing the K-band photometry of these 6 objects we find an offset of $0\overset{\rm m}{.}30$ with a standard deviation of $0\overset{\rm m}{.}67$; excluding one outlier at $\Delta(\mathrm{mag}) \simeq 1\overset{\rm m}{.}4$ the offset is reduced to $0\overset{\rm m}{.}09$ with a standard deviation of $0\overset{\rm m}{.}47$. The large offset is mainly due to the fact that Nagayama et al. derive isophotal magnitudes at a surface brightness of $20^{\rm m}$ per square arcsec (cf. previous section). In fact, their K-band photometry agrees well with the 2MASS K_{20} magnitudes.

7.4. 21 cm wavelength

A complementary way to find galaxies in the Galactic plane is through blind H I surveys, which have two major advantages: (i) the H I emission of the interstellar gas in galaxies is not affected by Galactic extinction; and (ii) the H I observation usually produces an accurate radial velocity. On the other hand, H I surveys miss elliptical and many lenticular galaxies, and at low Galactic latitude H I-faint galaxies may be missed due to the increased noise caused by strong Galactic continuum sources.

The blind H I Parkes ZoA survey, conducted with the multibeam receiver on the Parkes telescope (Staveley-Smith et al. 2000), surveyed the entire southern ZoA ($212° \le \ell \le 36°$, $|b| \le 5°$) in the velocity range -1200 to $12\,700$ km s^{-1} with an integration time of 25 min. We have extracted detections from two sub-surveys: (i) the shallow H I ZoA survey (hereafter HIZSS; Henning et al. 2000) comprises 8% of the integration time of the full survey and has a sensitivity of 15 mJy beam^{-1} after Hanning smoothing; (ii) Juraszek et al. (2000; hereafter JS00) have studied the area of the GA ($308° \lesssim \ell \lesssim 332°$) at 16% of the integration time of the full survey with a sensitivity of 20 mJy beam^{-1} before Hanning smoothing. The theoretical sensitivity after Hanning smoothing (~14 mJy beam^{-1}) is only marginally better than the one of the shallow survey despite the increase in integration time since the sensitivity depends on the longitude (continuum sources cause ripples in the H I spectra), and the GA region lies closer to the Galactic centre than the average field in the shallow survey.

There are 12 detections in total in the DENIS search area. They are shown in Fig. 9, where large open circles stand for the HIZSS survey and large open squares for JS00. Note that the position uncertainty is about 4 arcmin. Four galaxies were detected in common by the two surveys, and one HIZSS galaxy at $l = 307.46$, $b = 0.69$ was not detected by JS00 but appears in the full deep survey. Of the eight H I galaxies, four were detected with the DENIS survey, while the other four are neither visible in the blue nor in the NIR.

A discussion of the velocity distribution is given in Schröder et al. (2005) and Paper II.

8. Extinction and NIR colours

Colours of nearby galaxies, unaffected by k- and evolutionary corrections, are independent of distance. Hence, NIR colours can be used as an independent means to derive extinctions in

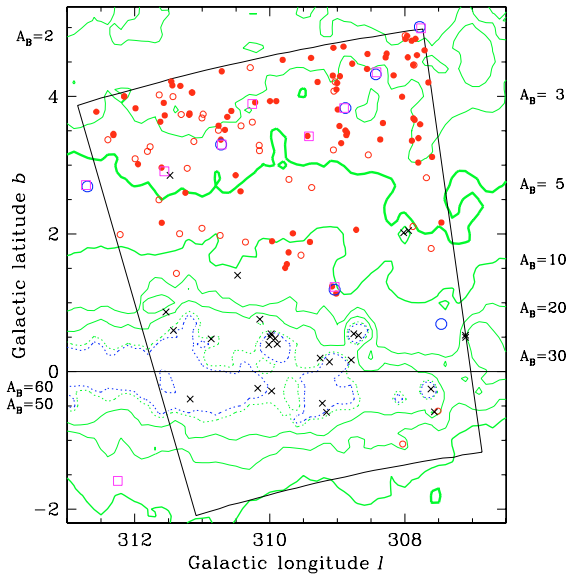

Fig. 9. Same as Fig. 3, but with galaxies detected with HIZSS (*large open circles*) and JS00 (*large open squares*) overlaid.

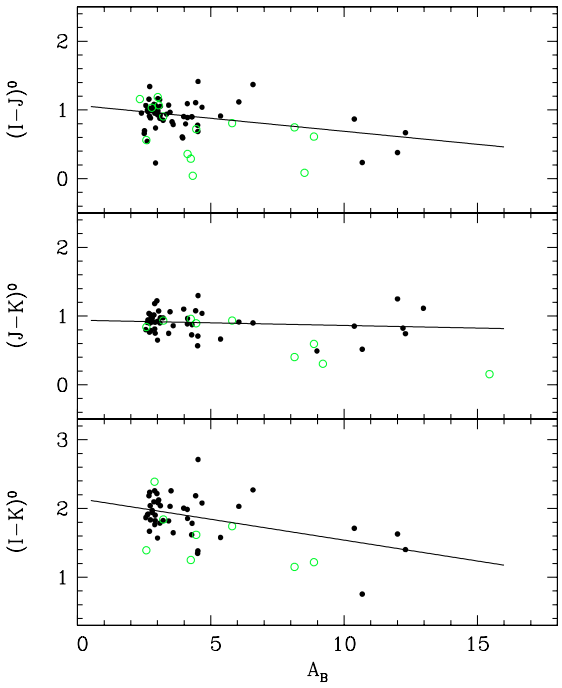

Fig. 10. The NIR colours, corrected for extinction according to the IRAS/DIRBE maps, are plotted versus extinction in the *B*-band. *Filled circles* are galaxies, while *open circles* are uncertain galaxies. The *line* represents the least squares fit to the filled circles only.

low latitude areas where the IRAS/DIRBE maps of Schlegel et al. (1998) are not properly calibrated. For our analysis we have applied the extinction correction according to the IRAS/DIRBE maps to all colours and look for dependencies in the residuals.

Figure 10 shows the results (filled circles are galaxies, open circles uncertain candidates): galaxies at higher extinctions are clearly too blue, i.e., *the extinctions of the IRAS/DIRBE maps are overestimated at low galactic latitudes*. The least squares fits to the filled circles (i.e., excluding the uncertain candidates) give:

$$(I-J)^0 = (-0.04\pm0.01)A_B + (1.07\pm0.06), \quad (2)$$

$$(J-K)^0 = (-0.01\pm0.01)A_B + (0.94\pm0.05), \quad (3)$$

$$(I-K)^0 = (-0.06\pm0.02)A_B + (2.15\pm0.09), \quad (4)$$

where the rms deviations of the data points from the best fit line are $\sigma = 0.21, 0.18$, and 0.28, respectively. A Spearman Rank test indicates probabilities of 0.11, 0.21, and 0.04 that the slopes of the fits in $I-J$, $J-K$, and $I-K$, occur by chance, respectively.

For a generic colour C, Eqs. (2)–(4) can be written as

$$C^0 = aA_B + b, \quad (5)$$

the reddening equation is simply

$$C = C^0 + \left(\frac{E}{A_B}\right)A_B, \quad (6)$$

and the true extinction-corrected colour is

$$\widetilde{C^0} = C - \left(\frac{E}{A_B}\right)\widetilde{A}_B. \quad (7)$$

Combining Eqs. (5)–(7), one gets

$$\widetilde{C^0} = a\,A_B + b + \left(A_B - \widetilde{A}_B\right)\left(\frac{E}{A_B}\right). \quad (8)$$

If the opacity is overestimated by some constant factor, that is, if the extinction, A_B, is overestimated by some constant additive term, there would be no slope in Fig. 10, i.e., $a = 0$ for $\widetilde{C^0}$ to be independent of A_B in Eq. (8).

We therefore now assume that the true extinction is a constant f times the IRAS/DIRBE value of Schlegel et al.:

$$\widetilde{A}_B = f\,A_B, \quad (9)$$

and that the selective extinctions in the DENIS bands given in Eqs. (1) (see Sect. 3) are exact (we use tilde signs for "true" quantities). Equation (8) becomes

$$\widetilde{C^0} = \left[a + (1-f)\left(\frac{E}{A_B}\right)\right]A_B + b, \quad (10)$$

so, for the extinction-corrected colour to be independent of $\widetilde{A}_B$, and hence A_B (from Eq. (9)), the quantity in brackets in Eq. (10) must be zero, yielding

$$f = 1 + \frac{a}{E/A_B}. \quad (11)$$

With the selective extinctions of Eqs. (1) and the a coefficients from Eqs. (2)–(4), Eq. (11) yields $f = 0.84 \pm 0.05$ using $I-J$, $f = 0.93 \pm 0.08$ using $J-K$, and $f = 0.83 \pm 0.05$ using $I-K$. Combining the first two, independent, estimates of f (see, e.g., Appendix A of Sanchis et al. 2004), we conclude that

$$\widetilde{A}_B = (0.87 \pm 0.04)\,A_B, \quad (12)$$

i.e., *in this area of the Galactic plane, the true reddening appears to be 13% lower than the IRAS/DIRBE estimate of Schlegel et al.*

8.1. Caveats

With a sample like the present one, where the uncertainties are large, it is important to understand the possible biases and different explanations for the effect seen. In the following we address the most important caveats.

8.1.1. Patchiness

One of the problems with attempting to calibrate the extinctions in the Galactic plane is the relatively poor spatial resolution of 6′ of the IRAS/DIRBE maps, which misses extinction variations on smaller angular scales. As a consequence it is possible that we miss galaxies in the high-extinction patches and therefore underestimate the overall true extinction.

We have tested this by restricting our least squares fit to the points below $A_B = 10^{\rm m}$, assuming that we find all galaxies around $A_B = 10^{\rm m}$ and that the variations in A_B are not very large (this is confirmed by the fact that no considerable changes in star counts in the I-band are apparent at these extinction levels). The least squares fits to our data of Fig. 10, restricted to $A_B < 10^{\rm m}$, now show considerably larger variations and errors:

$$(I-J)^0 = (+0.04 \pm 0.03)A_B + (0.83 \pm 0.11), \quad (13)$$

$$(J-K)^0 = (-0.04 \pm 0.02)A_B + (1.07 \pm 0.08), \quad (14)$$

$$(I-K)^0 = (-0.00 \pm 0.04)A_B + (1.95 \pm 0.16), \quad (15)$$

where the rms deviations of the data points from the best fit line are similar to the fit to the full range in extinction, namely σ = 0.20, 0.16, and 0.26, respectively. The resulting corrections for the extinction are now (Eq. (11)): $f = 1.15 \pm 0.13$ using $I-J$, $f = 0.64 \pm 0.17$ using $J-K$, and $f = 0.99 \pm 0.12$ using $I-K$. Combining the first two (independent) estimates of f, which are, however, not consistent anymore, we find

$$\widetilde{A}_B = (0.96 \pm 0.10)\, A_B. \quad (16)$$

Therefore, *the IRAS/DIRBE extinctions of Schlegel et al. are consistent with the NIR colours of the galaxies of our sample, restricted to* $A_B < 10^{\rm m}$.

The major drawback of this method is that our restricted sample has only very few galaxies above $A_B = 5^{\rm m}$ and none below $A_B = 2\overset{\rm m}{.}2$, hence, the range in extinctions is too small to provide meaningful fits. With a larger sample one could also compare the scatter in colour at low and at high extinctions: the scatter in colour at any given extinction is expected to be inflated by the uncertainty in the extinction correction; in other words, the extinctions would have considerably large error bars. A galaxy in a higher extinction patch would be redder than expected, and if we start missing galaxies at the highest extinctions it means we are biased towards the blue. We would therefore expect the scatter in colour to decrease at the high extinction end because we would miss more and more of the red galaxies and hence be biased towards the blue as the fits indicate.

We could test this on a different project, the search for NIR counterparts of galaxies found in a blind H I survey (Schröder et al. 2005). This sample covers the extinction range $1^{\rm m} < A_B < 8^{\rm m}$ with better statistics, and we do not find such a decrease in scatter. In fact, the dependence on extinction found in this project confirms our first result (Eq. (12)), i.e.,

$$\widetilde{A}_B = (0.79 \pm 0.05)\, A_B. \quad (17)$$

A comparison of the estimates of f for the colour $I-K$ gives more consistent results (the sample of galaxies here is slightly different and comprises only of galaxies with measurements in all three passbands): $f = 0.83 \pm 0.05$ from Eq. (4), and $f = 0.84 \pm 0.08$ from Schröder et al. (2005). The estimate of f from the low extinction sample, i.e., $f = 0.99 \pm 0.12$ (Eq. (15)), agrees within the errors.

We are therefore confident that the variation of the extinction on a small scale (the x-axis error) at these levels is small and does not affect our fit significantly.

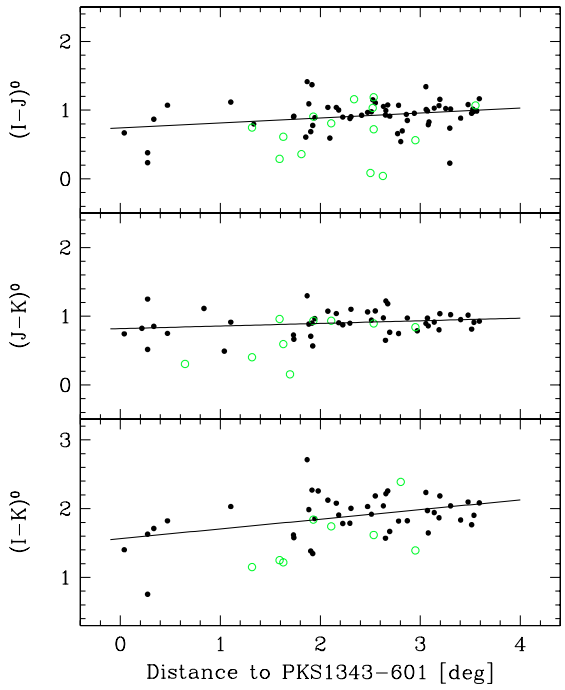

Fig. 11. The NIR colours, corrected for extinction according to the IRAS/DIRBE maps, as a function of distance from PKS 1343 – 601 in degrees. *Filled circles* are galaxies, while *open circles* are uncertain galaxies. The *line* represents the least squares fit to the filled circles.

8.1.2. Morphological segregation

Rich clusters usually show a morphological segregation: one finds predominantly early-type (red) galaxies in the centre and late-type (blue) galaxies in the outskirts of a cluster.

To investigate this we have plotted the colours corrected for extinction according to the IRAS/DIRBE maps as a function of *distance* to PKS 1343 – 601 in degrees (Fig. 11), assuming that PKS 1343 – 601 is at or very near the centre of the cluster.

Contrary to the expectation we find that the galaxies close to PKS 1343 – 601 are clearly bluer than those at a larger distance. However, since the cluster seems to be much smaller than expected (see Paper II where we derive a virial radius of $\sim 0\overset{\circ}{.}3$), we do not expect to see any colour change due to morphological segregation much beyond that. In fact, if we exclude the inner $0\overset{\circ}{.}6$ from the fit we do not find any significant dependence on distance anymore. On the other hand, we cannot achieve a proper fit using only the six galaxies within the inner $0\overset{\circ}{.}6$ since the scatter is too large. We therefore cannot determine whether we see a colour change due to morphological segregation.

To explain why the inner six galaxies are bluer than the rest we refer to Fig. 3 which shows that these galaxies are all located at the highest extinction levels where we still find galaxies. In other words, Fig. 11 shows only the extinction effect seen in Fig. 10 in a slightly different form. To demonstrate this, we have corrected the colours for the extinction as determined in Eq. (12), and Fig. 12 with the corrected colours shows no further dependence on extinction, i.e., the slopes are now consistent with zero. No difference can be seen between the galaxies within the virial radius and the rest, and we conclude that any possible effect of morphological segregation does not affect our fit significantly.

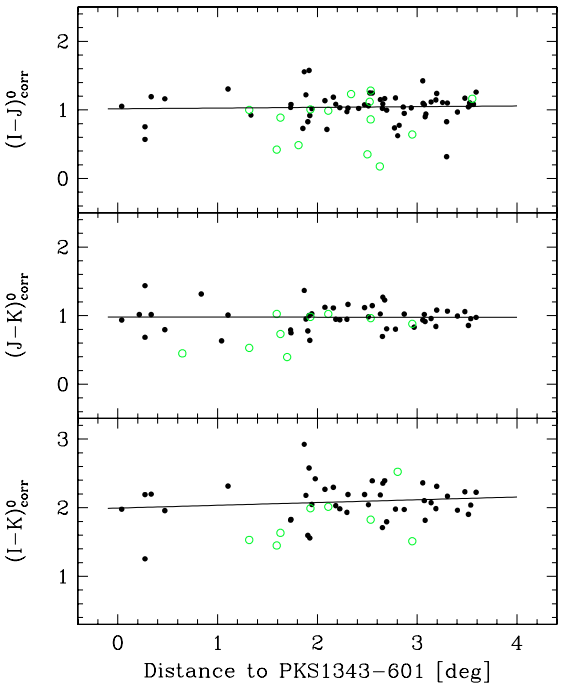

Fig. 12. Same as Fig. 11, but with a correction factor of $f = 0.87$ applied to the extinctions.

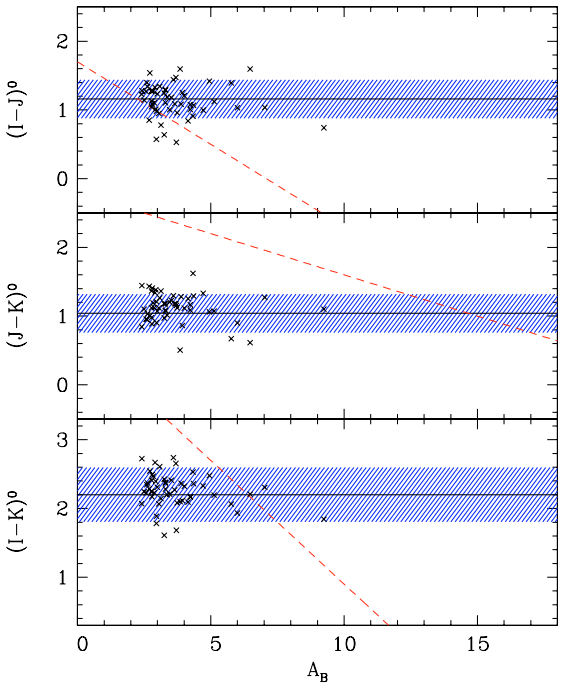

Fig. 13. Monte Carlo simulation of galaxies with their extinction-corrected colours displayed in the same format as Fig. 10. The dashed lines indicate the limiting colour above which faint galaxies will be missed; the shaded regions depict the 1σ-distributions of the intrinsic colours.

8.1.3. Survey magnitude limits

The limiting magnitude of the DENIS survey depends on the passband, see Sect. 2. As a consequence we will start losing red and faint galaxies when the observed (extincted) colour approaches the difference between the limiting magnitudes. We therefore expect a bias towards blue galaxies at higher extinctions, exactly as we see in Fig. 10.

To investigate the extent of this effect (since only the faint galaxies are affected) we performed a series of Monte Carlo simulations of a sample of galaxies subjected to different extinctions. The galaxy magnitudes were selected from a Euclidean galaxy count function (cf. Fig. 1) using the magnitude limits for galaxies given in Sect. 2; the (intrinsic) colour distribution was assumed to be Gaussian around mean colours. The galaxy positions were taken from a uniform distribution of galactic latitudes, and extinctions were derived by a cubic spline fit between observed latitudes and extinctions. The resulting extinction corrected colours were then plotted versus extinction to imitate Fig. 10 and a slope was fitted.

Mean colours and their distributions have been determined by one of us (G. Mamon, to be published) for a large sample of high-latitude and bright DENIS galaxies ($|b| > 60°$) using `SExtractor`. Mean colours and dispersions were derived using the following selection criteria: `SExtractor` flag 0, distance from image border >50 pixel, and three passes on magnitude limits: (1) magnitude limits as given in Sect. 2, (2) $J < 12 + \langle J-K\rangle_{\rm pass1} - 0.5$, $I < 12 + \langle J-K\rangle_{\rm pass1} + \langle I-J\rangle_{\rm pass1} - 1$, and (3) restricting to $\pm 0\overset{\rm m}{.}5$ from $\langle{\rm colour}\rangle_{\rm pass2}$. While the 2nd pass allows for a J (I) cut that is essentially complete in K (J), the 3rd pass removes interlopers (rare stars incorrectly classified as galaxies). Using the same aperture as in the present work (7″) he found the following means and sigma:

$$\langle I-J\rangle = 1.16 \pm 0.14, \quad (18)$$

$$\langle J-K\rangle = 1.04 \pm 0.14. \quad (19)$$

Using these input parameters we find for 1000 simulations (using 5000 galaxies each as input which resulted in a similar number of galaxies "detected" as in reality) that a slope of −0.04 (−0.01, and −0.06) as observed in Fig. 10 is observed 0.7% (40%, and 0.6%) of the time by chance for $I-J$ ($J-K$, and $I-K$), respectively, assuming that the Schlegel et al. extinctions are correct. We can therefore say that this extinction overestimate by Schlegel et al. that we find in the colours $I-J$ and $I-K$ is statistically significant, while on the other hand the low slope for $J-K$ indicates a low sensitivity to extinction and is not significant.

One of the simulations is shown in Fig. 13, which is given in the same format as Fig. 10: the 1σ colour distributions are indicated as well as the (observed) colour at the magnitude limits (that is, beyond these limits we lose faint galaxies). It is quite obvious that the line in $I-J$ intersects the galaxy colours already at extinctions of $A_B \simeq 2^{\rm m}$. It is therefore not possible to simply avoid this bias by restricting the fit to the lower extinction ranges.

We also investigated how sensitive these results are to a deviation in the NIR galaxy colours, which depend on the precise selective transmission of the telescope optics, filter, and detector, as well as galaxy type and aperture size. Jarrett et al. (2003) find a mean $J-K$ colour of $1\overset{\rm m}{.}0$ for galaxies in the 2MASS survey with some variations depending on galaxy type. Mamon's sample of bright high-latitude DENIS galaxies shows a variation in $I-J$ with aperture, so that the largest aperture, 40″, gives $\langle I-J\rangle = 1.04$ with incidentally the smallest dispersion, 0.11. Extracting the DENIS catalogue of LEDA galaxies (Paturel et al. 2005), we made a selection based on type = G, $|b| > 60°$, all 12 flags (4 per band times 3 bands) = 0 (good quality), and using the same magnitude passes as described above for Mamon's sample, we find $1\overset{\rm m}{.}06 \pm 0.14$ and $0\overset{\rm m}{.}96 \pm 0.19$ for $\langle I-J\rangle$ and $\langle J-K\rangle$, respectively. It should be noted that these colours

refer to the total magnitudes; and due to the higher sensitivity in the blue bands of the DENIS survey, the colours are biased towards the blue. Finally, Mamon et al. (1998) find $1\overset{\mathrm{m}}{.}15$ and $1\overset{\mathrm{m}}{.}05$ for bright high latitude DENIS galaxies, while our galaxy sample, after correction for the effect seen in Fig. 10, gives $1\overset{\mathrm{m}}{.}07$ and $0\overset{\mathrm{m}}{.}98$, respectively (Eqs. (2) and (3)).

We therefore also tested a set of bluer colours ($1\overset{\mathrm{m}}{.}00$ and $0\overset{\mathrm{m}}{.}95$ with the same dispersion as in the first test). The simulations show that 1.6% (38%, and 0.7%) of the slopes are more negative than observed in Fig. 10. The $I - J$ result is slightly more significant than the result for the redder colours, but it should be stressed that these numbers are very extreme. The *uncertainty* in intrinsic colour, therefore, does not have a very large effect on the slopes.

Hence, we conclude that despite uncertainties in the mean intrinsic colours the simulations show that the overestimate of extinction by Schlegel et al. that we find is statistically significant given the magnitude selection effects.

8.2. Discussion

We have shown that in our search area the extinction estimates of the DIRBE/IRAS maps by Schlegel et al. (1998) are slightly overestimated, which cannot be fully explained by (i) patchiness of the extincting material in the sky; (ii) morphological segregation within the assumed cluster; or (iii) selection effects at the magnitudes limits of the survey.

While the fractional error in the reddening estimates of the DIRBE/IRAS maps is 16% (Schlegel et al.), we find a systematic overestimation of $1/f = 15\%$ ($f = 0.87$), thus fairly large in comparison with the DIRBE/IRAS uncertainty on a single point. When comparing reddening values derived from Mg_2 indices of a large sample of elliptical galaxies, Schlegel et al. find that the highest reddening values of their maps appear to be overestimated. Inspecting their Fig. 6 we can say that a slope of $f - 1 = -0.13$ according to our findings is compatible with their data. It has to be stressed, though, that the sparsity of points at $E(B-V) > 0.2$ in their figure makes it difficult to estimate a slope at all. Schlegel et al. state clearly (in their Appendix C) that their predicted reddenings at low Galactic latitudes ($|b| < 5°$) are not to be trusted because of (i) the possibility that contaminating sources may exist (our search area is such a case though no such sources have been found by us), and (ii) a calibration at higher extinctions was not attempted.

Since then, various attempts have been made to calibrate the DIRBE/IRAS maps at different latitudes and using different objects and methods. Most of these find that the DIRBE/IRAS maps are overestimated at low latitudes.

Nagayama et al. (2004), who have also searched for galaxies in this cluster (see Sect. 7.3), have determined extinction values using $J - K$ colours of foreground giant stars. They find that the extinction in the K-band, A_K, is systematically lower by $0\overset{\mathrm{m}}{.}4$ than the DIRBE/IRAS values. This corresponds to a factor of $f \simeq 0.67$ for the average extinction in this area. Their extinction map shows a higher spatial resolution than the DIRBE/IRAS maps, and one can see that the variation of their extinction along a line of equal extinction in the DIRBE/IRAS maps is only moderate ($\sigma(A_K) \simeq 0\overset{\mathrm{m}}{.}3$). This indicates that the intrinsic patchiness in this area does not lead to large variations in extinction on a small spatial scale and hence has not caused us to predominantly miss galaxies in supposedly very high extinction patches (see Sect. 8.1.1).

Dutra et al. (2003b) have derived reddening values from the spectral continuum in the optical of elliptical galaxies in three different areas of the sky. In combination with previous work by this group (Dutra et al. 2003a), where they used bulge giants within 10 degrees of the Galactic centre to derive an A_K extinction map, they find a calibration factor of $f \sim 0.75$ for reddening values of up to $E(B - V) = 1.6$ ($A_B = 6\overset{\mathrm{m}}{.}6$).

Choloniewski & Valentijn (2003b) used the surface brightness of galaxies in the ESO-LV catalogue (Lauberts & Valentijn 1989) in the R- and B-band (Choloniewski & Valentijn 2003a) and find a calibration factor of $f = 0.71$.

Other work in the literature include Arce & Goodman (1999), who find $0.67 < f < 0.77$ for reddening in the Taurus dark cloud complex, and Schröder et al. 2005 with $f = 0.79$, as discussed in Sect. 8.1.1. On the other hand, Fingerhut et al. 2003 find a much *higher* extinction in the direction of Maffei 1, which translates to $f = 1.3$. However, this is a single object and seems to be the exception.

We can therefore conclude that our calibration factor of $f = 0.87$ derived from a fairly high extinction area ($2^{\mathrm{m}} \lesssim A_B \lesssim 12^{\mathrm{m}}$) is in reasonable agreement with the results of other investigations ($0.67 < f < 0.79$) at various extinction levels in the sense that the DIRBE/IRAS maps overestimate the extinction at low Galactic latitudes where they are uncalibrated. Though in some cases a higher R_V could explain the overestimation (e.g., work done in the blue bands or in high density clouds), the NIR is fairly insensitive to R_V. Hence, our results in the NIR cannot be explained by a nonstandard reddening law.

We have shown that there is no obvious evidence that we predominately find galaxies in low extinction patches in the investigated range of extinctions, but better statistics are needed to completely solve this question. One possible way would be to use galaxies at moderate extinction levels (where we can be sure to go reasonably deep to find all galaxies in the NIR) in an area of high spatial density of galaxies, e.g., the Norma cluster in the centre of the GA region, to look for a strong spatial variation in the reddening estimates by other means. One could also investigate larger areas by comparing shallow surveys with deeper ones, e.g., using the UKIDSS (Lawrence 2006) and VISTA (McPherson et al. 2003) projects, to determine whether the fainter "new" galaxies in the deeper surveys show all significantly larger reddening values. In fact, the comparison of our "shallow" search with the deeper search by Nagayama (2004) already indicates that a strong spatial variation cannot be the only explanation: the shallow survey finds actually a higher absolute extinction than the deeper one, contrary to the argument for patchiness.

However, independent of the cause, a calibration factor of about $f = 0.87$ applied to the DIRBE/IRAS maps will improve significantly the actual extinction correction for galaxies at low latitudes.

9. Conclusion

We have investigated a ~30 square-degree area around the radio-bright galaxy PKS 1343 – 601 using the NIR survey DENIS. We found 83 galaxies and 39 possible candidates. The searched area covers a wide range of extinctions (from $\sim 2^{\mathrm{m}}$ to over 100^{m} where the search area crosses the Galactic plane). The galaxy counts reflect the dependence on extinction, as qualitatively shown in Fig. 1 (i.e., the effect is less pronounced for the longer wavelengths), as well as the underlying large-scale structures: there is a clear enhancement of galaxies around the radio galaxy, indicating that there is a cluster or at least a group of galaxies.

Our detections compare well with those of the 2MASS survey: while we find more galaxies at intermediate extinctions due

to the I-band, which is more sensitive to late-type spiral galaxies than the J- and K-bands, 2MASS goes deeper in the K-band. However, our search is more reliable, since the 2MASS extended source catalogue is derived automatically and includes both galaxies and extended objects in our Galaxy without distinction.

Using the NIR galaxy colours from the 7″ aperture, we find that the extinction derived from the IRAS/DIRBE maps (Schlegel et al. 1998) is overestimated by about 15%; that is, the ratio of true extinction as derived using NIR colours to IRAS/DIRBE extinction is $f = \widetilde{A_B}/A_B = 0.87 \pm 0.04$. Other findings in the literature confirm this result.

We investigated several possible explanations: (i) patchiness of obscuring material which results in our finding galaxies only in areas of below-average extinction; (ii) morphological segregation within the dense system of galaxies around PKS 1343 – 601; and (iii) selection effects at the magnitudes limits of the survey. None of these affect the galaxy colours presented here on a statistical significant level. We therefore conclude that the poor calibration of the IRAS/DIRBE at low latitudes is the major cause of the overestimate.

Since our work is nearly independent of R_V (we use the same R_V to calculate extinctions as Schlegel et al. used to calculate $E(B-V)$), the disagreement cannot be explained by a nonstandard reddening law. Also, a variation in the dust temperature along the line of sight, which is very likely, would lead to an underestimate of the IRAS/DIRBE extinction (Schlegel et al. 1998) and can therefore not be the explanation either.

The second paper of this series (Schröder & Mamon 2006) will discuss the question whether PKS 1343 – 601 is part of a cluster or a mere group of galaxies, making use of the galaxy distribution, velocity distribution, and X-ray emission.

Acknowledgements. The authors are grateful to the DENIS teams in Chile and at PDAC for all thir efforts in observing and reducing the data, in particular J. Borsenberger, G. Simon, P. Texier for preferential treatment of the DENIS data needed for this project. We thank Ch. Motch for making unpublished data available to us.

The DENIS project has been partly funded by the SCIENCE and the HCM plans of the European Commission under grants CT920791 and CT940627. It is supported by INSU, MEN, and CNRS in France, by the State of Baden-Württemberg in Germany, by DGICYT in Spain, by CNR in Italy, by FFwFBWF in Austria, by FAPESP in Brazil, by OTKA grants F–4239 and F–013990 in Hungary, and by the ESO C&EE grant A–04–046. This research has made use of the NASA/IPAC Infrared Science Archive (2MASS) and the NASA/IPAC Extragalactic Database (NED), which are operated by the Jet Propulsion Laboratory, California Institute of Technology, under contract with the National Aeronautics and Space Administration, as well as the Lyon-Meudon Extragalactic Database (LEDA), supplied by the LEDA team at the Centre de Recherche Astronomique de Lyon, Obs. de Lyon. Furthermore, this research has also made use of the Digitized Sky Surveys (produced at the Space Telescope Science Institute under US Government grant NAG W-2166) and the SuperCOSMOS Sky Surveys (produced by the Wide Field Astronomy Unit at the University of Edinburgh). A. Schröder gratefully acknowledges financial support from the European Marie Curie Fellowship Grant.

Appendix A: Photometry

We have tested the quality of the photometry by matching all objects extracted by `SExtractor` in the overlap regions between (a) images within one slot (overlap in Dec), (b) images of adjacent slots (overlap in RA), and (c) re-observations of the same slot (overlap of the whole images). Figure A.1 shows a sketch of these overlap regions in exaggerated form. The matching was done automatically and was only possible for observations where high quality astrometry was available (see Col. 10 in Table 1). For each pair of strips we have then plotted the differences in the total magnitudes as well as in the 7″-aperture magnitudes for the matched objects versus magnitude, time, RA, and Dec (the latter two depend on the kind of overlap regions) to look for systematic dependences.

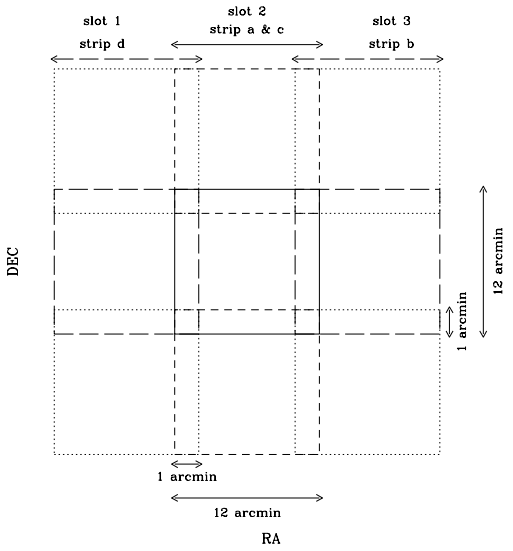

Fig. A.1. The different overlap regions of an image are shown here in exaggerated form. Each image of slot 2 has been observed twice (strips a and c). There are 1-arcmin-wide overlap regions in RA (between adjacent slots) and in Dec (between images of the same strip).

In the following we will discuss the results in detail. A summary of the global effects of photometric and seeing conditions on the photometry of each strip is given in Table 1.

- We used the magnitude differences of matched objects in the RA overlap regions, plotted versus time (i.e., scan direction), to look for variation in atmospheric extinction. These can be distinguished from normal scatter by the fact that they occur in all three passbands with the same amplitude. Abrupt changes as small as $\Delta\mathrm{mag} = 0\overset{\mathrm{m}}{.}1$ were immediately obvious (e.g., strip 9426), while other strips showed a constant significant offset over the whole range of images (about 12 min observing time), e.g., strip 3823.
- Bad seeing conditions can also show rapid variations of the magnitude difference versus time, but in this case the 7″-aperture magnitudes are much more strongly affected than the total magnitudes, and there are marked differences between the passbands (e.g., strip 9461).
- In the I-band a small number of points show an offset of $\pm\sim 0\overset{\mathrm{m}}{.}25$ from the mean for the following strips: 7659, 9426, 3625, 7747, 6371, 7462, 7532, 7484, 3976. A simple check on the images showed that the affected objects were scattered among the "normal" objects in the overlap region. There seems to be a dependence on RA in such a way that the left quarter to half of the image is not affected. No dependence on Dec across the image could be found. No apparent reason for such deviations could be found.
- Small but negligible variations in the magnitude differences due to the pattern of the 2×2 CCDs that make the image could be found both in RA and Dec.
- Occasionally an increased scatter for the very brightest objects was found, mainly due to saturation.
- Small offsets of the mean magnitude difference in the Dec overlap regions within a strip indicate a slight gradient across an image.
- For strips between ~6000 and ~7800, the J-band shows a marked lack of points in the RA overlap region in two places: just to the right of the middle of the image, and in

the right-hand corner. This was due to the lack of detections by SExtractor around black areas in the CCDs.

A total recalibration of all the observations in the survey is planned by PDAC which will remove most of the intrinsic effects that we have noticed.

References

Abell, G. O. 1958, ApJS, 3, 211
Arce, H. G., & Goodman, A. A. 1999, ApJ, 512, L135
Arp, H. C., & Madore, B. F. 1987, A Catalog of Southern Peculiar Galaxies and Associations (Cambridge: Cambridge University Press)
Bertin, E., & Arnouts, S. 1996, A&AS, 117, 393
Borsenberger, J. 1997, in The Impact of Large-Scale Near-IR Sky Surveys, ed. F. Garzón, N. Epchtein, A. Omont, B. Burton, & P. Persi (Dordrecht: Kluwer), 181
Cameron, L. M. 1990, A&A, 233, 16
Cardelli, J. A., Clayton, G. C., & Mathis, J. S. 1989, ApJ, 345, 245
Choloniewski, J., & Valentijn, E. A. 2003a, Acta Astron., 53, 249
Choloniewski, J., & Valentijn, E. A. 2003b, Acta Astron., 53, 265
Dekel, A. 1994, ARA&A, 32, 371
Dutra, C. M., Santiago, B. X., Bica, E. L. D., & Barbuy, B. 2003a, MNRAS, 338, 253
Dutra, C. M., Ahumada, A. V., Clariá, J. J., Bica, E., & Barbuy, B. 2003b, A&A, 408, 287
Ebeling, H., Mullis, C. R., & Tully, R. B. 2002, ApJ, 580, 774
Elvis, M., Wilkes, B. J., McDowell, J. C., et al. 1994, ApJS, 95, 1
Epchtein, N. 1997, in The Impact of Large Scale Near-IR Surveys, ed. F. Garzón, N. Epchtein, A. Omont, B. Burton, & P. Persi (Dordrecht: Kluwer), 15
Epchtein, N. 1998, in 179th Symp. of the IAU, New Horizons from Multi-Wavelength Sky Surveys, ed. B. J. McLean, D. A. Golombek, J. J. E. Hayes, & H. E. Payne (Dordrecht: Kluwer), 106
Epchtein, N., Batz, B. de, Capoani, L., et al. 1997, Messenger, 87, 27
Fairall, A. P., Woudt, P. A., ed. 2005, Nearby Large-Scale Structures & the Zone of Avoidance (San Francisco: ASP), ASP Conf. Ser., 329
Fingerhut, R. L., McCall, M. L., De Robertis, M., et al. 2003, ApJ, 587, 672
Forman, W., Jones, C., Cominsky, L., et al. 1978, ApJS, 38, 357
Gandhi, P., & Fabian, A. C. 2003, MNRAS, 339, 1095
Gardner, J. P., Sharples, R. M., Carrasco, B. E., & Frenk, C. S. 1996, MNRAS, 282, L1
Girardi, M., Mardirossian, F., Marinoni, C., Mezzetti, M., & Rigoni, E. 2003, A&A, 410, 461
Griffith, M. R., Wright, A. E., Burke, B. F., & Ekers, R. D. 1994, ApJS, 90, 179
Hambly, N. C., MacGillivray, H. T., Read, M. A., et al. 2001, MNRAS, 326, 1279
Henning, P. A., Staveley-Smith, L., Ekers, R. D., et al. 2000, AJ, 119, 2686 (HIZSS)
Henning, P. A., Kraan-Korteweg, R. C., & Staveley-Smith, L. 2005, in Nearby Large-Scale Structures and the Zone of Avoidance (San Francisco: ASP), ASP Conf. Ser., 199
Jarrett, T.-H., Chester, T., Cutri, R., et al. 2000a, AJ, 119, 2498
Jarrett, T.-H., Chester, T., Cutri, R., et al. 2000b, AJ, 120, 298
Jarrett, T.-H., Chester, T., Cutri, R., Schneider, S., & Huchra, J. P. 2003, AJ, 125, 525
Joint *IRAS* Science Working Group 1988, *IRAS* Point Source Catalog, Version 2 (Washington: US Govt. Printing Office) (IRAS PSC)
Jones, P. A., Lloyd, B. D., & McAdam, W. B. 2001, MNRAS, 325, 817
Joye, W. A., & Mandel, E. 2003, in Astronomical Data Analysis Software and Systems XII, ed. H. E. Payne, R. I. Jedrzejewski, & R. N. Hook (San Francisco: ASP), ASP Conf. Ser., 295, 489
Juraszek, S. J., Staveley-Smith, L., Kraan-Korteweg, R. C., et al. 2000, AJ, 119, 1627 (JS00)
Karachentseva, V. E., & Karachentsev, I. D. 2000, A&AS, 146, 359
Kolatt, T., Dekel, A., & Lahav, O. 1995, MNRAS, 275, 797
Kraan-Korteweg, R. C. 2000, A&ASS, 141, 123
Kraan-Korteweg, R. C. 2005, in From Cosmological Structures to the Milky Way, Rev. Modern Astronomy 18, ed. S. Röser (New York: Wiley), 48
Kraan-Korteweg, R. C., Woudt, P. A., Cayatte, V., et al. 1996, Nature, 379, 51
Kraan-Korteweg, R. C., Schröder, A., Mamon, G. A., & Ruphy, S. 1998, in 3rd Euroconference, The Impact of Near IR Surveys, ed. N. Epchtein (Dordrecht: Kluwer), 209
Kraan-Korteweg, R. C., & Woudt, P. A. 1999, PASA, 16, 53
Kraan-Korteweg, R. C., & Lahav, O. 2000, A&ARv, 10, 211
Kraan-Korteweg, R. C., & Jarrett, T. H. 2005, in Nearby Large-Scale Structures and the Zone of Avoidance (San Francisco: ASP), ASP Conf. Ser., 119
Kraan-Korteweg, R. C., Ochoa, M., Woudt, P., & Andernach, H. 2005a, in Nearby Large-Scale Structures and the Zone of Avoidance (San Francisco: ASP), ASP Conf. Ser., 159
Kraan-Korteweg, R. C., Staveley-Smith, L., Donley, J., Koribalski, B., & Henning, P. A. 2005b, in IAU Symp. 216, Maps of the Cosmos, ed. M. Colless, & L. Staveley-Smith (San Francisco: ASP), ASP Conf. Ser., 203
Lauberts, A., & Valentijn, E. A. 1989, The Surface Photometry Catalogue of the ESO-Uppsala Galaxies, (Garching: ESO)
Lawrence, A., Warren, S. J., Almaini, O., et al. 2006, MNRAS, submitted [arXiv:astro-ph/0604426]
Lynden-Bell, D., Faber, S. M., Burstein, D., et al. 1988, ApJ, 326, 19
Mamon, G. A. 1994, in Unveiling Large-Scale Structures Behind the Milky Way, ed. C. Balkowski, & R. C. Kraan-Korteweg (San Francisco: ASP), ASP Conf. Ser., 67, 53
Mamon, G. A. 1998, in XIVth IAP Astrophysics Meeting, Wide Field Surveys in Cosmology, ed. S. Colombi, Y. Mellier, & B. Raban (Gif-sur-Yvette: Éditions Frontières), 323
Mamon, G. A., Borsenberger, J., Tricottet, M., & Banchet, V. 1998, in 3rd Euroconference, The Impact of Near IR Surveys, ed. N. Epchtein (Dordrecht: Kluwer), 177
Mamon, G. A. 2000, in Cosmic Flows 1999: Towards an Understanding of Large-Scale Structure, ed. S. Courteau, M. A. Strauss, & J. A. Willick (San Francisco: ASP), ASP Conf. Ser., 201, 103
Mamon, G. A., Parker, Q. A., & Proust, D. 2001, PASA, 18, 232
Masetti, N., Pretorius, M. L., Palazzi, E., et al. 2006, A&A, 449, 1139
McAdam, W. B. 1991, PASA, 9, 255
McPherson, A. M., Craig, S. C., & Sutherland, W. 2003, Large Ground-based Telescopes, ed. J. M. Oschmann, & L. M. Stepp, Proc. of the SPIE, 4837, 82
Michel, L., Herent, O., Motch, C., et al. 2004, in Astronomical Data Analysis Software and Systems (ADASS) XIII, ed. F. Ochsenbein, M. G. Allen, & D. Egret (San Francisco: ASP), ASP Conf. Ser., 314, 570
Monnier Ragaigne, D., van Driel, W., Schneider, S. E., Jarrett, T. H., & Balkowski, C. 2003, A&A, 405, 99
Moriondo, G., Baffa, C., Casertano, S., et al. 2001, A&A, 370, 881
Motch, C., Herent, O., & Guillot, P. 2003, Astr. Nachr., 324, 61
Nagayama, T., Woudt, P. A., Nagashima, C., et al. 2004, MNRAS, 354, 980
Paturel, G., Petit, C., Rousseau, J., & Vauglin, I. 2003, A&A, 405, 1
Paturel, G., Vauglin, I., Petit, C., et al. 2005, A&A, 430, 751
Piconcelli, E., Sánchez-Portal, M., Guainazzi, M., et al. 2006, A&A, 453, 839
Rembold, S. B., Pastoriza, M. G., Ducati, J. R., Rubio, M., & Roth, M. 2002, A&A, 391, 531
Rousseau, J., Paturel, G., Vauglin, I., et al. 2000, A&A, 363, 62
Sanchis, T., Mamon, G. A., Salvador-Solé, E., & Solanes, J. M. 2004, A&A, 418, 393
Schlegel, D. J., Finkbeiner, D. P., & Davis, M. 1998, ApJ, 500, 525
Schröder, A., Kraan-Korteweg, R. C., Mamon, G. A., & Ruphy, S. 1997, in XVIIth Moriond Astrophysics Meeting, Extragalactic Astronomy in the Infrared, ed. G. A. Mamon, Trinh Xuân Thuân, & J. Trân Thanh Vân (Gif-sur-Yvette: Éditions Frontières), 381
Schröder, A., Kraan-Korteweg, R. C., & Mamon, G. 1999, PASA, 16, 42
Schröder, A., Kraan-Korteweg, R. C., & Mamon, G. 2000, in Mapping the Hidden Universe: The Universe behind the Milky Way – The Universe in HI (San Francisco: ASP), ASP Conf. Ser., 218, 119
Schröder, A., Mamon, G., Kraan-Korteweg, R. C., & Woudt, P. A. 2005, in Nearby Large-Scale Structures & the Zone of Avoidance, ed. A. P. Fairall, & P. A. Woudt (San Francisco: ASP), ASP Conf. Ser., 329, 167
Schröder, A., & Mamon, G. 2007, A&A, submitted (Paper II)
Skrutskie, M. F., Cutri, R. M., Stiening, R., et al. 2006, AJ, 131, 116
Staveley-Smith, L., Koribalski, B. S., Stewart, I., et al. 2000, in Imaging at Radio through Submillimetre Wavelengths, ed. J. G. Mangum, & S. J. E. Radford (San Francisco: ASP), ASP Conf. Ser., 217, 50
Tashiro, M., Kaneda, H., Makishima, K., et al. 1998, ApJ, 499, 713
Two Micron All Sky Survey team 2003, 2MASS extended objects. Final release
Vauglin, I., Paturel, G., Borsenberger, J., et al. 1999, A&AS, 135, 133
Watson, M. G., Auguéres, J.-L., Ballet, J., et al. 2001, A&A, 365, L51
West, R. M., & Tarenghi, M. 1989, A&A, 223, 61
Woudt, P. A., & Kraan-Korteweg, R. C. 2001, A&A, 380, 441 (WKK)
Woudt, P. A., Fairall, A. P., Kraan-Korteweg, R. C., et al. 2005, in Nearby Large-Scale Structures and the Zone of Avoidance, ed. A. P. Fairall, & P. A. Woudt (San Francisco: ASP), ASP Conf. Ser., 329, 147
Wright, A., & Otrupcek, R. 1990, Parkes Catalog, Australia telescope national facility
XMM-Newton Survey Science Centre (SSC) 2003, The First XMM-Newton Serendipitous Source Catalogue, Version 1 (1XMM)

Online Material

Appendix B: Images of Galactic objects

Thumbnail images of the Galactic nebulae, presented and discussed in Sect. 6.2, are displayed in Fig. B.1. They are available in the electronic form of the journal. There are two objects per row, each with the *I*-, *J*-, and *K*-band image shown from left to right; the name is printed at the top and the total *B*-band extinction and Galactic coordinates at the bottom of the images. The *J*- and *K*-band images have been smoothed, and the cut values have been calculated separately for each image depending on the background.

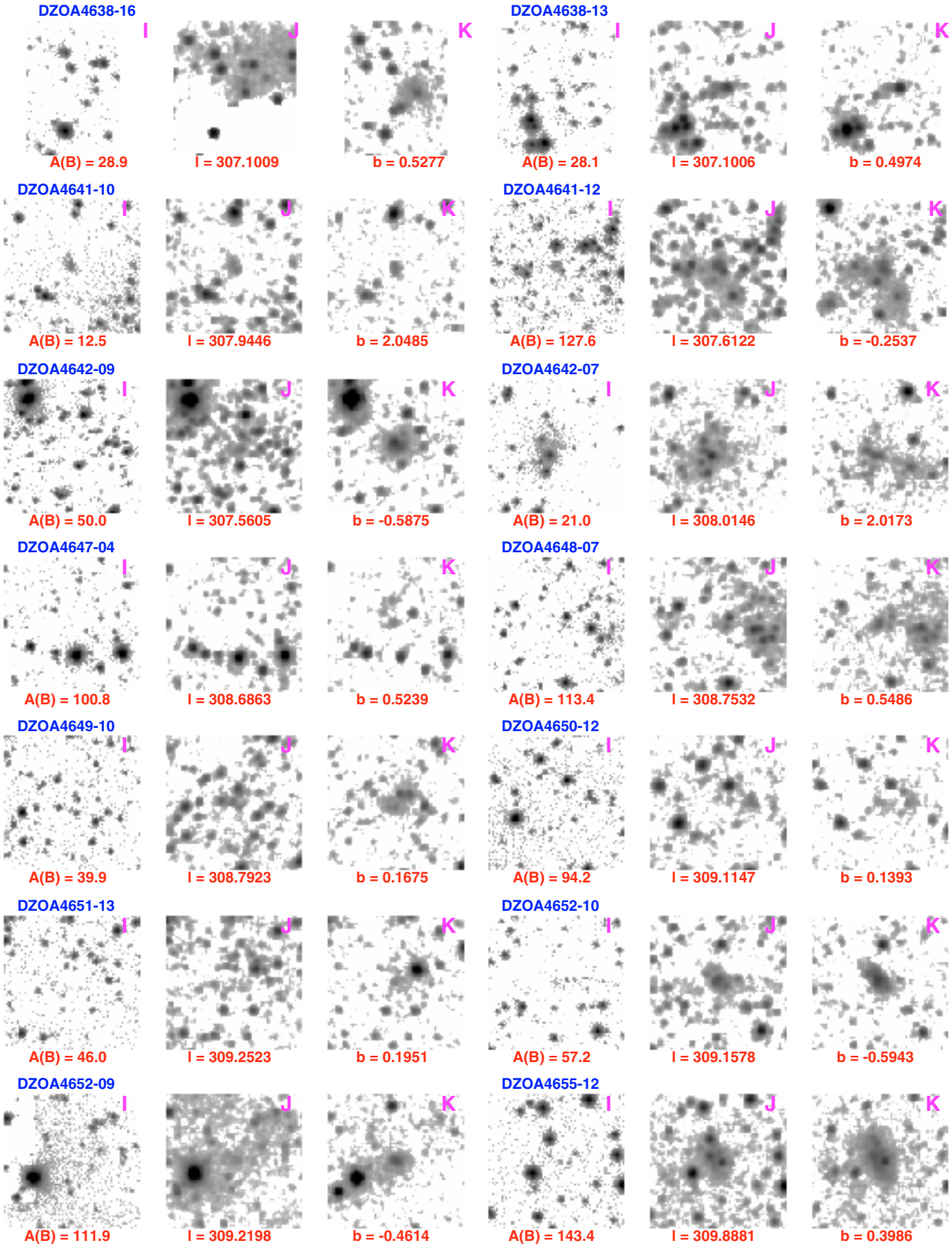

Fig. B.1. *I*-, *J*-, and *K*-band images (*left, middle, and right hand column*, respectively) of the Galactic nebulae discussed in Sect. 6.2; names, total *B*-band extinctions, and Galactic coordinates are given for each set. The minimum and maximum cut values for the *I*-band are 1.0 and 300, respectively, for the *J*-band they are 0.05 and 70, respectively, and for the *K*-band they are 0.1 and 70, respectively.

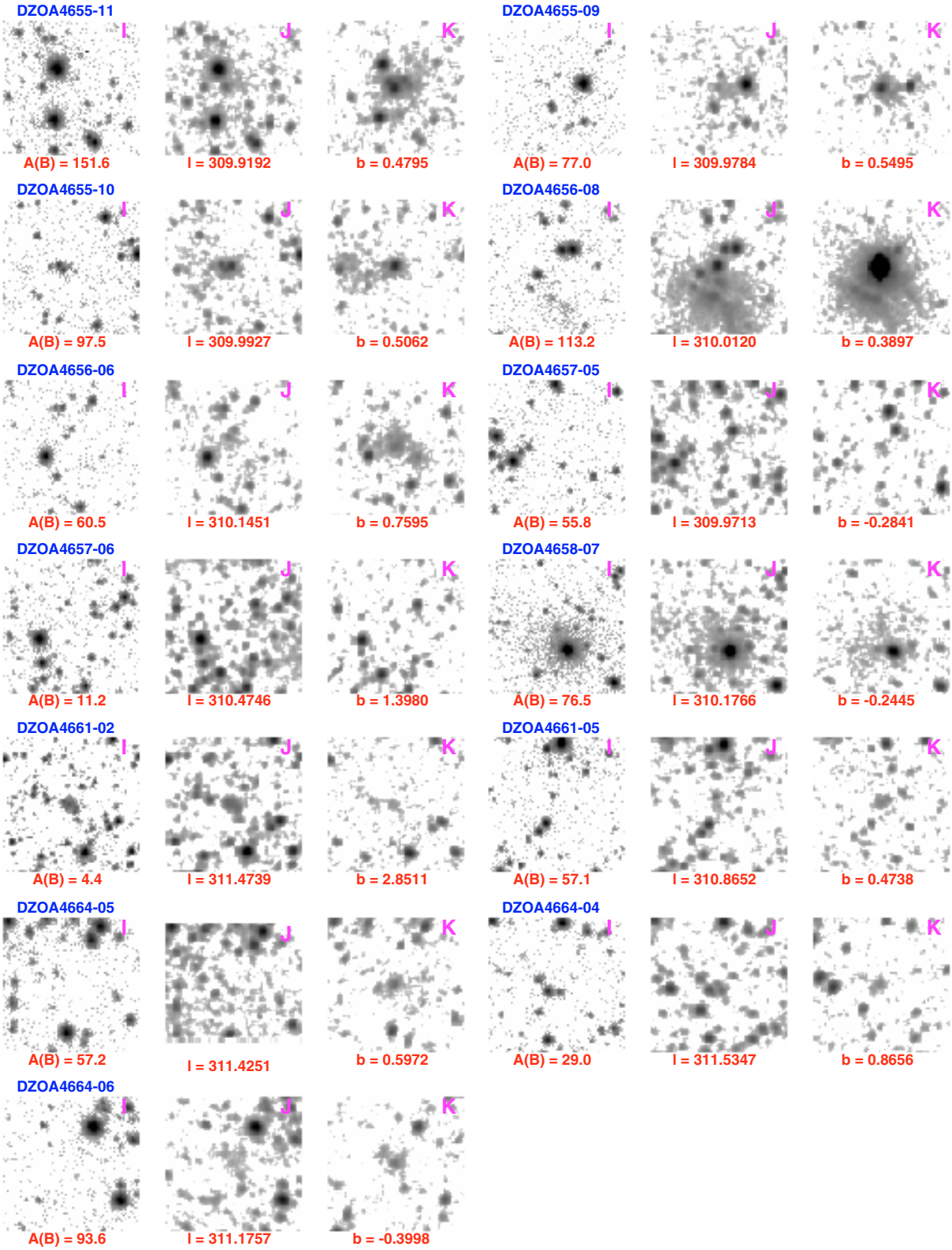

Fig. B.1. continued.

Table 2. Galaxies in the search area.

Ident.	N	RA (J2000) [h m s]	Dec [° ′ ″]	Gal ℓ [°]	Gal b [°]	A_B [mag]	Class	Visibil.	Type	I [mag]	J [mag]	K [mag]	$(I-J)^0$ [mag]	$(I-K)^0$ [mag]	$(J-K)^0$ [mag]	Phot.	D_I [″]	D_J [″]	D_K [″]
(1)	(2)	(3a)	(3b)	(4a)	(4b)	(5)	(6)	(7)	(8)	(9)	(10)	(11)	(12)	(13)	(14)	(15)	(16)	(17)	(18)
DZOA4638-04	1	13 27 20.3	–57 52 08	307.71	4.67	2.8	*DG*	0 1 1 1	SM	15.35 ± 0.10	13.87 ± 0.06	... ...	1.01 ± 0.10	... ...	... ...	000	11	14	5
DZOA4638-09	1	13 27 25.1	–58 20 28	307.65	4.20	2.6	*DG*	0 1 1 1	E/SE	15.96 ± 0.07	14.02 ± 0.06	12.87 ± 0.28	1.06 ± 0.09	1.87 ± 0.20	0.80 ± 0.19	030	11	12	7
DZOA4638-03	1	13 28 10.0	–57 41 09	307.84	4.83	3.0	*DG*	0 1 1 1	E/SE	16.10 ± 0.08	14.19 ± 0.06	12.98 ± 0.27	1.17 ± 0.09	2.08 ± 0.18	0.93 ± 0.17	000	10	13	5
DZOA4638-11	1	13 28 10.3	–60 22 59	307.46	2.17	5.0	*DG*	0 1 1 1	SM	13.70 ± 0.02	11.92 ± 0.02	10.90 ± 0.06	0.27 ± 0.02	0.83 ± 0.04	0.56 ± 0.04	774	17	35	15
DZOA4638-10	2	13 28 11.0	–59 25 09	307.60	3.12	3.1	*DG*	0 1 1 0	SM	16.40 ± 0.08	... ...	... ...	... ...	... ...	... ...	000	10	8	...
DZOA4638-06	2	13 28 15.4	–57 55 21	307.82	4.60	2.7	*DG*	0 1 1 1	SM	15.64 ± 0.05	14.19 ± 0.05	12.65 ± 0.25	0.88 ± 0.07	1.83 ± 0.23	0.95 ± 0.23	000	10	12	6
DZOA4638-01	2	13 28 37.1	–57 42 19	307.90	4.81	2.9	*DG*	1 1 1 1	SE	13.96 ± 0.01	12.02 ± 0.02	10.78 ± 0.05	0.98 ± 0.02	1.90 ± 0.04	0.91 ± 0.04	000	22	25	17
DZOA4639-07	3	13 28 44.4	–58 03 32	307.87	4.46	2.8	*UG*	0 1 1 0	SM	... ...	... ...	... ...	... ...	... ...	... ...	000	7	8	...
DZOA4639-06	1	13 28 49.7	–58 03 21	307.88	4.46	2.7	*DG*	1 1 1 1	SM	15.48 ± 0.06	14.05 ± 0.06	... ...	1.02 ± 0.09	... ...	... ...	330	10	12	7
DZOA4639-19	2	13 29 00.3	–58 55 30	307.77	3.59	2.6	*BG*	1 1 1 0	SL	... ...	15.27 ± 0.18	... ...	... ...	... ...	... ...	000	6	9	...
DZOA4639-02	1	13 29 01.7	–57 37 32	307.97	4.88	3.0	*DG*	0 1 1 0	SM	16.30 ± 0.15	14.95 ± 0.13	... ...	0.99 ± 0.17	... ...	... ...	000	7	6	...
DZOA4639-14	1	13 29 10.4	–59 42 27	307.68	2.82	4.1	*UG*	0 1 1 0	S	... ...	... ...	... ...	... ...	... ...	... ...	000	6	7	...
DZOA4639-01	1	13 29 14.7	–57 37 06	308.00	4.88	3.0	*UG*	0 1 1 1	E/SE	16.93 ± 0.12	14.71 ± 0.09	... ...	1.07 ± 0.16	... ...	... ...	000	9	13	7
DZOA4639-03	1	13 29 16.1	–57 39 56	307.99	4.83	2.9	*DG*	0 1 1 1	SM	15.79 ± 0.06	13.60 ± 0.05	12.99 ± 0.25	0.95 ± 0.09	1.77 ± 0.22	0.81 ± 0.22	030	12	15	6
DZOA4639-05	2	13 29 17.7	–57 56 03	307.96	4.57	2.7	*DG*	1 1 1 1	E/SE	14.30 ± 0.01	12.20 ± 0.02	11.20 ± 0.07	1.02 ± 0.02	2.04 ± 0.04	1.02 ± 0.04	040	20	22	14
DZOA4639-10	1	13 29 25.8	–59 07 11	307.80	3.39	2.6	*DG*	0 1 1 1	E/SE	15.51 ± 0.05	13.53 ± 0.05	12.61 ± 0.22	0.98 ± 0.07	1.92 ± 0.16	0.94 ± 0.16	000	10	10	7
DZOA4639-09	1	13 29 33.2	–58 50 54	307.86	3.66	3.0	*DG*	1 1 1 1	SM	14.25 ± 0.03	12.39 ± 0.03	11.39 ± 0.14	0.93 ± 0.05	1.57 ± 0.13	0.65 ± 0.13	330	17	25	11
DZOA4639-08	1	13 29 40.9	–58 49 30	307.87	3.68	3.1	*DG*	0 1 1 1	SE	... ...	... ...	12.65 ± 0.15	... ...	... ...	... ...	000	15	13	7
DZOA4639-16	6	13 29 50.5	–60 44 05	307.61	1.79	5.8	*UG*	0 1 1 1	SM	16.15 ± 0.06	13.83 ± 0.03	12.48 ± 0.10	0.81 ± 0.09	1.74 ± 0.10	0.93 ± 0.08	300	6	9	8
DZOA4639-13	3	13 29 51.9	–59 28 19	307.80	3.04	3.1	*DG*	1 1 1 1	SM	15.57 ± 0.03	13.48 ± 0.03	12.50 ± 0.12	0.88 ± 0.04	1.79 ± 0.09	0.90 ± 0.09	440	11	12	8
DZOA4640-05	2	13 30 13.4	–59 08 34	307.90	3.35	3.1	*DG*	0 1 1 1	SE	15.96 ± 0.07	14.45 ± 0.07	... ...	0.92 ± 0.10	... ...	... ...	000	9	12	6
DZOA4640-03	2	13 30 34.6	–58 29 24	308.04	3.99	3.4	*DG*	1 1 1 1	SE	15.51 ± 0.06	13.64 ± 0.05	12.86 ± 0.21	1.07 ± 0.08	1.82 ± 0.16	0.75 ± 0.16	000	13	14	8
DZOA4640-02	2	13 31 09.6	–58 09 45	308.17	4.30	2.8	*DG*	0 1 1 1	E	14.35 ± 0.02	12.69 ± 0.02	11.79 ± 0.09	0.95 ± 0.03	1.74 ± 0.07	0.79 ± 0.07	740	17	18	12
DZOA4641-01	1	13 31 33.3	–57 50 04	308.27	4.62	2.7	*DG*	1 1 1 1	SM	13.53 ± 0.02	11.52 ± 0.02	10.70 ± 0.07	1.16 ± 0.03	2.19 ± 0.05	1.04 ± 0.05	000	40	42	21
DZOA4641-04	1	13 31 36.6	–60 22 37	307.88	2.11	5.8	*UG*	0 0 1 1	SM	... ...	... ...	12.22 ± 0.22	... ...	... ...	0.79 ± 0.15	074	...	10	6
DZOA4641-02	1	13 31 43.7	–57 53 11	308.28	4.57	2.8	*DG*	1 1 1 1	E	13.64 ± 0.02	11.83 ± 0.01	10.57 ± 0.06	1.03 ± 0.02	1.94 ± 0.04	0.91 ± 0.04	000	20	23	14
DZOA4641-06	2	13 32 03.3	–63 05 06	307.51	–0.57	38.5	*UG*	0 0 0 1	?	... ...	... ...	12.25 ± 0.08	... ...	... ...	... ...	000	...	...	7
DZOA4642-04	2	13 33 11.8	–58 49 22	308.32	3.61	4.0	*DG*	1 1 1 1	SL	16.22 ± 0.08	14.26 ± 0.06	12.57 ± 0.24	0.84 ± 0.10	2.02 ± 0.18	1.18 ± 0.18	000	10	14	8
DZOA4642-01	2	13 33 39.2	–57 47 42	308.55	4.62	2.8	*DG*	1 1 1 1	SE	13.50 ± 0.02	11.47 ± 0.01	10.13 ± 0.06	1.04 ± 0.02	1.95 ± 0.04	0.91 ± 0.04	000	28	30	19
DZOA4642-06	2	13 33 47.6	–59 03 07	308.36	3.37	4.0	*DG*	1 1 1 1	SE/M	16.13 ± 0.07	14.24 ± 0.06	... ...	0.63 ± 0.10	... ...	... ...	030	9	9	6
DZOA4642-02	6	13 33 58.2	–58 00 29	308.56	4.40	3.2	*DG*	1 1 1 1	SE	14.16 ± 0.01	12.97 ± 0.01	11.22 ± 0.02	0.85 ± 0.01	1.83 ± 0.03	0.98 ± 0.03	330	27	33	22
DZOA4644-04	14	13 35 26.0	–59 14 38	308.54	3.15	4.1	*UG*	0 1 1 1	SM	15.60 ± 0.03	14.13 ± 0.03	... ...	0.36 ± 0.05	... ...	... ...	000	12	13	7
DZOA4644-02	6	13 35 30.1	–57 53 47	308.78	4.47	3.3	*DG*	0 1 1 0	SL	15.97 ± 0.09	14.33 ± 0.15	... ...	0.94 ± 0.15	... ...	... ...	000	9	8	...
DZOA4644-01	3	13 36 08.1	–57 37 48	308.91	4.72	2.7	*DG*	0 1 1 1	SE	16.29 ± 0.15	15.02 ± 0.22	... ...	1.01 ± 0.18	... ...	... ...	300	7	9	6
DZOA4645-01	2	13 37 05.0	–58 02 40	308.96	4.29	3.1	*DG*	0 1 1 1	SE	15.89 ± 0.05	14.08 ± 0.05	12.29 ± 0.20	1.05 ± 0.07	2.04 ± 0.17	0.98 ± 0.17	000	11	11	6
DZOA4645-14	2	13 37 15.2	–57 37 11	309.06	4.71	2.7	*BG*	1 1 1 0	SM/L	... ...	... ...	... ...	... ...	... ...	... ...	000	4	5	...
DZOA4645-13	2	13 37 20.7	–63 28 12	308.03	–1.05	24.3	*UG*	0 0 1 1	?	... ...	... ...	10.44 ± 0.05	... ...	... ...	... ...	006	...	8	15
DZOA4645-09	2	13 37 24.7	–58 52 21	308.86	3.47	4.5	*DG*	1 1 1 1	SE	13.10 ± 0.01	11.32 ± 0.01	10.28 ± 0.04	0.69 ± 0.01	1.38 ± 0.02	0.71 ± 0.02	000	47	43	22
DZOA4645-04	2	13 37 31.9	–58 08 01	309.00	4.19	3.1	*DG*	0 1 1 1	E	16.59 ± 0.07	14.59 ± 0.07	... ...	1.15 ± 0.09	... ...	... ...	000	9	9	6
DZOA4645-08	2	13 37 32.8	–58 50 04	308.88	3.50	4.5	*DG*	1 1 1 1	SL	15.00 ± 0.03	12.65 ± 0.03	12.38 ± 0.24	0.78 ± 0.05	1.35 ± 0.12	0.57 ± 0.12	003	17	22	10
DZOA4645-10	4	13 37 32.9	–58 54 14	308.87	3.44	4.5	*DG*	0 1 1 1	SM	14.29 ± 0.02	11.87 ± 0.01	10.56 ± 0.03	1.41 ± 0.02	2.71 ± 0.02	1.30 ± 0.02	000	24	30	18
DZOA4645-03	2	13 37 44.1	–58 06 37	309.03	4.21	3.0	*UG*	0 1 1 1	E/SE	16.75 ± 0.17	14.82 ± 0.12	... ...	1.19 ± 0.13	... ...	... ...	000	7	6	4
DZOA4645-05	2	13 37 44.3	–58 13 26	309.01	4.10	3.5	*DG*	1 1 1 0	SL	... ...	... ...	... ...	... ...	... ...	... ...	000	9	15	5
DZOA4645-02	2	13 37 51.3	–58 00 59	309.06	4.30	2.9	*DG*	0 1 1 0	S	17.13 ± 0.13	... ...	... ...	... ...	... ...	... ...	000	6	6	...
DZOA4645-07	3	13 37 59.2	–58 30 55	308.99	3.81	4.7	*DG*	0 1 1 1	SM/L	15.82 ± 0.06	12.52 ± 0.02	11.11 ± 0.06	1.04 ± 0.05	2.08 ± 0.07	1.04 ± 0.05	030	12	20	13
DZOA4646-01	6	13 38 03.3	–58 14 27	309.05	4.08	3.5	*UG*	0 1 1 1	SM	... ...	... ...	13.33 ± 0.18	... ...	... ...	... ...	000	7	9	5
DZOA4646-03	6	13 38 08.5	–58 45 19	308.97	3.57	4.1	*DG*	0 1 1 1	SE	14.33 ± 0.01	12.21 ± 0.01	11.11 ± 0.04	0.89 ± 0.01	1.85 ± 0.03	0.96 ± 0.03	000	17	19	17
DZOA4646-04	1	13 38 16.6	–59 00 15	308.94	3.32	4.3	*DG*	0 1 1 1	SE/M	15.74 ± 0.06	14.11 ± 0.05	12.72 ± 0.11	0.90 ± 0.07	1.62 ± 0.16	0.73 ± 0.15	000	12	15	6
DZOA4646-06	1	13 38 21.7	–60 17 02	308.72	2.06	9.0	*DG*	0 1 1 1	E/SE	... ...	13.77 ± 0.07	12.41 ± 0.18	... ...	... ...	0.49 ± 0.14	040	7	10	9
DZOA4647-03	4	13 39 17.6	–59 04 46	309.06	3.22	4.2	*UG*	0 1 1 1	SM/L	15.56 ± 0.03	13.89 ± 0.03	12.26 ± 0.14	0.29 ± 0.04	1.25 ± 0.11	0.96 ± 0.12	000	10	11	7
DZOA4647-01	2	13 39 39.7	–58 04 00	309.29	4.21	3.5	*DG*	0 1 1 1	SM	16.03 ± 0.06	13.76 ± 0.06	12.43 ± 0.22	0.97 ± 0.09	2.03 ± 0.17	1.06 ± 0.17	000	10	12	5
DZOA4647-02	1	13 39 52.7	–57 42 17	309.39	4.56	2.6	*DG*	1 1 1 1	SE	15.20 ± 0.06	13.80 ± 0.06	... ...	0.54 ± 0.08	... ...	... ...	000	12	14	5
DZOA4649-02	3+	13 41 54.8	–58 48 28	309.44	3.42	3.9	*DG*	0 1 1 1	SL	15.86 ± 0.08	13.32 ± 0.04	... ...	0.61 ± 0.12	... ...	... ...	000	25	25	6
DZOA4649-07	3+	13 42 09.8	–61 08 18	309.02	1.13	12.0	*DG*	0 0 1 1	?	... ...	... ...	... ...	... ...	... ...	... ...	000	...	17	15
DZOA4649-06	2+	13 42 29.6	–61 01 23	309.08	1.24	13.0	*DG*	0 0 1 1	SE	... ...	13.69 ± 0.05	11.31 ± 0.04	... ...	... ...	1.11 ± 0.07	000	...	14	13

Table 2. continued.

Ident.	N	RA (J2000) Dec		Gal ℓ	Gal b	A_B	Class	Visibil.	Type	I	J	K	$(I-J)^0$	$(I-K)^0$	$(J-K)^0$	Phot.	D_I	D_J	D_K
		[h m s]	[° ′ ″]	[°]	[°]	[mag]				[mag]	[mag]	[mag]	[mag]	[mag]	[mag]		[″]	[″]	[″]
(1)	(2)	(3a)	(3b)	(4a)	(4b)	(5)	(6)	(7)	(8)	(9)	(10)	(11)	(12)	(13)	(14)	(15)	(16)	(17)	(18)
DZOA4649-03	2+	13 42 35.6	–59 33 18	309.38	2.67	6.7	*UG*	0 1 1 0	SM/L	16.98 ± 0.17	... ...	... ...	... ...	... ...	... ...	000	5	6	...
DZOA4649-01	2	13 42 59.9	–57 39 06	309.81	4.53	2.5	*DG*	1 1 1 1	SM	15.69 ± 0.06	... ...	... ...	... ...	... ...	... ...	000	13	13	7
DZOA4650-09	1+	13 44 03.7	–60 19 35	309.40	1.88	10.4	*DG*	0 1 1 1	E/SE	16.67 ± 0.13	12.64 ± 0.03	10.61 ± 0.04	0.87 ± 0.14	1.71 ± 0.14	0.85 ± 0.06	003	5	24	16
DZOA4650-01	2+	13 44 36.5	–58 13 10	309.90	3.93	3.9	*DG*	0 1 1 1	SM	14.98 ± 0.03	... ...	... ...	... ...	... ...	... ...	377	18	20	11
DZOA4651-05	1	13 45 00.2	–59 22 17	309.72	2.79	6.2	*UG*	0 1 1 0	SM/L	... ...	... ...	... ...	... ...	... ...	... ...	000	2	3	...
DZOA4651-02	1	13 45 17.7	–58 12 01	310.00	3.93	3.5	*DG*	0 1 1 0	SL	... ...	14.88 ± 0.15	... ...	... ...	... ...	... ...	000	13	12	...
DZOA4651-08	1	13 45 25.3	–60 29 14	309.54	1.69	11.9	*UG*	0 0 1 1	?	... ...	... ...	11.80 ± 0.09	... ...	... ...	... ...	003	...	12	12
DZOA4651-06	2	13 45 50.7	–60 09 05	309.66	2.01	8.2	*DG*	0 1 1 1	E/SE	... ...	... ...	10.73 ± 0.06	... ...	... ...	... ...	004	12	21	13
DZOA4652-01	1	13 46 40.3:	–57 39 50:	310.29	4.42	2.3	*UG*	0 1 1 1	SE/M	16.16 ± 0.09	... ...	... ...	... ...	... ...	... ...	000	9	8	5
DZOA4652-04	2	13 46 48.9:	–60 24 29:	309.72	1.73	12.3	*DG*	0 1 1 1	E	15.74 ± 0.05	11.62 ± 0.01	9.11 ± 0.02	0.67 ± 0.05	1.40 ± 0.05	0.74 ± 0.02	000	12	38	32
DZOA4652-02	1	13 46 57.3:	–58 10 19:	310.22	3.91	3.3	*DG*	0 1 1 0	SL	17.26 ± 0.17	... ...	... ...	... ...	... ...	... ...	000	5	7	...
DZOA4653-09	4	13 47 18.5	–60 34 13	309.75	1.56	12.2	*DG*	0 0 1 1	SE/M	... ...	12.65 ± 0.02	10.24 ± 0.02	... ...	... ...	0.82 ± 0.04	000	...	22	21
DZOA4653-03	1	13 47 32.3	–58 47 45	310.16	3.29	3.8	*UG*	0 1 1 0	?	... ...	... ...	... ...	... ...	... ...	... ...	000	10	8	...
DZOA4653-11	1	13 47 36.2	–60 37 04	309.77	1.51	12.0	*DG*	0 1 1 1	Sy 2	16.77 ± 0.13	13.14 ± 0.04	10.56 ± 0.06	0.38 ± 0.14	1.63 ± 0.14	1.25 ± 0.05	000	7	14	16
DZOA4653-04	1	13 47 38.2	–58 52 15	310.15	3.21	4.3	*UG*	0 1 1 0	S	... ...	... ...	... ...	... ...	... ...	... ...	000	4	2	...
DZOA4653-01	1	13 47 44.1	–58 26 38	310.26	3.62	3.8	*UG*	0 1 1 1	SM	... ...	... ...	... ...	... ...	... ...	... ...	000	15	17	10
DZOA4653-07	1	13 48 27.5	–60 11 47	309.97	1.89	10.7	*DG*	0 1 1 1	S	16.23 ± 0.09	13.29 ± 0.04	11.46 ± 0.07	0.24 ± 0.11	0.75 ± 0.12	0.52 ± 0.08	030	8	18	11
DZOA4654-03	1	13 49 04.0	–58 27 34	310.43	3.57	3.2	*UG*	0 1 1 1	SM	15.65 ± 0.07	13.92 ± 0.11	12.16 ± 0.19	0.91 ± 0.11	1.84 ± 0.19	0.93 ± 0.19	403	9	11	8
DZOA4654-02	1	13 49 46.1	–58 13 04	310.57	3.79	2.6	*DG*	1 1 1 1	SM	14.61 ± 0.04	12.96 ± 0.04	11.81 ± 0.14	1.00 ± 0.06	1.91 ± 0.11	0.91 ± 0.11	000	16	16	10
DZOA4654-01	1	13 49 49.9	–57 37 25	310.71	4.36	2.5	*DG*	1 1 1 0	SL	16.34 ± 0.12	14.59 ± 0.11	... ...	0.66 ± 0.21	... ...	... ...	000	12	7	...
DZOA4655-01	1+	13 50 21.3	–58 17 12	310.63	3.70	2.9	*DG*	0 1 1 1	SE	14.91 ± 0.05	13.15 ± 0.05	12.51 ± 0.14	1.07 ± 0.05	1.82 ± 0.11	0.75 ± 0.10	330	14	14	8
DZOA4655-04	1+	13 50 47.0	–59 23 08	310.43	2.62	6.1	*DG*	0 1 1 1	SM	15.59 ± 0.13	12.86 ± 0.06	11.70 ± 0.12	1.12 ± 0.11	2.03 ± 0.13	0.91 ± 0.09	033	12	15	12
DZOA4655-03	1+	13 50 55.3	–59 08 29	310.51	2.85	4.1	*DG*	0 1 1 1	SM/L	15.70 ± 0.08	13.82 ± 0.06	... ...	0.80 ± 0.12	... ...	... ...	000	12	9	8
DZOA4655-02	1+	13 50 56.5	–58 27 46	310.66	3.51	3.5	*DG*	0 1 1 1	SM	15.88 ± 0.08	... ...	12.21 ± 0.11	... ...	2.26 ± 0.14	... ...	000	13	12	8
DZOA4655-08	1+	13 51 03.5	–57 47 15	310.83	4.17	2.5	*BG*	1 0 0 0	SL	... ...	... ...	... ...	... ...	... ...	... ...	000	...	...	...
DZOA4656-01	1	13 51 31.9	–58 23 01	310.76	3.57	3.0	*DG*	0 1 1 1	SE	15.75 ± 0.09	13.64 ± 0.07	12.85 ± 0.19	1.04 ± 0.12	2.12 ± 0.19	1.07 ± 0.18	000	8	12	7
DZOA4656-04	1	13 51 33.9	–60 07 17	310.36	1.88	9.2	*UG*	0 1 1 1	S	... ...	13.45 ± 0.05	12.21 ± 0.20	... ...	... ...	0.31 ± 0.15	030	7	9	8
DZOA4656-03	2	13 51 38.6	–58 35 15	310.72	3.37	4.1	*DG*	1 1 1 1	SE	12.77 ± 0.01	10.81 ± 0.01	9.14 ± 0.01	1.09 ± 0.01	1.99 ± 0.01	0.89 ± 0.01	000	48	54	37
DZOA4656-02	1	13 51 39.8	–58 26 48	310.76	3.51	3.2	*UG*	0 1 0 0	SM/L	... ...	... ...	... ...	... ...	... ...	... ...	000	5	...	...
DZOA4657-03	1	13 52 55.4	–58 09 59	310.99	3.74	2.3	*UG*	0 1 1 1	E/SE	15.94 ± 0.09	14.61 ± 0.12	... ...	1.16 ± 0.14	... ...	... ...	000	6	9	5
DZOA4657-04	1	13 53 08.7	–58 12 59	311.00	3.69	2.4	*UG*	0 1 1 0	SL	... ...	... ...	... ...	... ...	... ...	... ...	000	8	8	5
DZOA4657-02	1	13 53 32.4	–57 49 30	311.15	4.05	2.7	*DG*	0 1 1 1	E/SE	... ...	... ...	... ...	... ...	... ...	... ...	000	12	11	7
DZOA4657-01	1	13 53 34.1	–57 49 10	311.15	4.06	2.7	*DG*	0 1 1 1	SE	14.81 ± 0.04	13.26 ± 0.04	12.25 ± 0.14	0.91 ± 0.04	1.67 ± 0.10	0.77 ± 0.10	000	15	14	9
DZOA4658-06	1	13 54 18.1:	–59 56 14:	310.74	1.98	10.1	*UG*	0 1 1 0	S	17.69 ± 0.18	14.28 ± 0.15	... ...	0.57 ± 0.20	... ...	... ...	999	4	8	...
DZOA4658-04	1	13 54 23.1:	–58 06 30:	311.19	3.75	2.5	*DG*	0 1 1 1	SM	... ...	... ...	... ...	... ...	... ...	... ...	999	9	12	8
DZOA4658-03	1	13 54 27.3:	–58 07 35:	311.19	3.73	2.6	*DG*	1 1 1 1	SM	14.68 ± 0.03	12.69 ± 0.04	... ...	1.49 ± 0.06	... ...	... ...	999	14	15	12
DZOA4658-01	1	13 54 38.5:	–57 41 11:	311.32	4.15	2.3	*DG*	1 1 1 0	SE	... ...	... ...	... ...	... ...	... ...	... ...	999	4	6	...
DZOA4658-05	1	13 54 39.5:	–58 31 07:	311.12	3.34	3.4	*UG*	0 1 1 1	SM	17.48 ± 0.12	14.38 ± 0.09	... ...	1.42 ± 0.20	... ...	... ...	999	6	9	3
DZOA4659-13	2	13 55 18.4	–58 05 32	311.31	3.74	2.8	*UG*	0 1 1 1	E/SE	15.84 ± 0.13	14.48 ± 0.12	... ...	1.03 ± 0.13	... ...	... ...	000	9	9	5
DZOA4659-11	1	13 55 29.0	–57 38 59	311.44	4.16	2.4	*BG*	1 1 1 0	SE/M	15.80 ± 0.09	14.48 ± 0.10	... ...	0.95 ± 0.17	... ...	... ...	300	6	13	3
DZOA4659-10	1	13 55 29.5	–57 35 26	311.46	4.22	2.4	*BG*	1 1 1 0	S	... ...	... ...	... ...	... ...	... ...	... ...	000	5	3	...
DZOA4659-01	1	13 55 43.5	–57 48 38	311.43	4.00	2.9	*UG*	0 1 1 1	–	15.99 ± 0.07	13.04 ± 0.04	11.50 ± 0.15	1.24 ± 0.09	2.39 ± 0.15	1.15 ± 0.14	060	4	8	5
DZOA4659-02	1	13 56 07.7	–58 52 21	311.22	2.95	3.8	*UG*	0 1 1 1	?	14.75 ± 0.03	13.21 ± 0.04	13.09 ± 0.22	0.52 ± 0.05	0.88 ± 0.18	0.37 ± 0.18	664	11	17	6
DZOA4659-05	1	13 56 09.7	–59 46 14	311.00	2.08	8.1	*UG*	0 1 1 1	S	16.85 ± 0.17	13.64 ± 0.05	12.65 ± 0.17	0.75 ± 0.14	1.15 ± 0.19	0.40 ± 0.15	000	10	10	5
DZOA4660-02	1	13 56 52.3	–57 51 53	311.57	3.91	2.5	*DG*	1 1 1 1	SM	15.98 ± 0.08	14.50 ± 0.08	... ...	0.70 ± 0.13	... ...	... ...	000	10	12	6
DZOA4660-05	1	13 57 01.5	–59 12 35	311.25	2.60	5.4	*DG*	0 1 1 1	E/SE	15.86 ± 0.06	13.05 ± 0.04	11.91 ± 0.13	0.91 ± 0.07	1.58 ± 0.11	0.67 ± 0.10	030	10	14	15
DZOA4660-03	1	13 57 06.7	–58 02 43	311.55	3.72	2.9	*DG*	0 1 1 1	E/SE	16.22 ± 0.08	14.00 ± 0.06	12.98 ± 0.23	1.08 ± 0.10	2.26 ± 0.16	1.18 ± 0.15	000	9	12	8
DZOA4660-01	2	13 57 08.2	–57 44 09	311.63	4.02	2.6	*UG*	0 1 1 1	SE	15.05 ± 0.03	13.94 ± 0.04	13.13 ± 0.20	0.56 ± 0.05	1.39 ± 0.16	0.84 ± 0.16	000	12	13	6
DZOA4660-04	1	13 57 46.6	–58 07 01	311.62	3.63	3.0	*DG*	0 1 1 1	E	15.51 ± 0.06	13.98 ± 0.06	12.20 ± 0.15	0.99 ± 0.06	2.22 ± 0.10	1.22 ± 0.10	000	9	10	9
DZOA4661-03	2	13 58 52.6	–59 45 47	311.33	2.00	8.9	*UG*	0 1 1 1	S	17.16 ± 0.09	13.91 ± 0.04	12.68 ± 0.12	0.66 ± 0.10	1.26 ± 0.13	0.59 ± 0.09	030	4	9	7
DZOA4661-01	2	13 58 57.0	–58 46 02	311.60	2.96	4.3	*DG*	1 1 1 1	SM	13.99 ± 0.01	11.44 ± 0.01	10.05 ± 0.02	0.95 ± 0.01	1.81 ± 0.02	0.86 ± 0.02	030	26	27	22
DZOA4662-02	2	13 59 35.7:	–58 25 49:	311.77	3.27	4.5	*UG*	0 1 1 1	E/SE	15.35 ± 0.03	13.35 ± 0.06	12.09 ± 0.09	0.72 ± 0.04	1.62 ± 0.07	0.90 ± 0.07	400	10	12	11
DZOA4662-03	1	14 00 01.9:	–58 29 06:	311.81	3.20	4.9	*UG*	0 1 1 0	S	16.71 ± 0.11	... ...	... ...	... ...	... ...	... ...	000	10	7	...
DZOA4662-01	1	14 00 04.0:	–57 50 02:	311.99	3.83	2.7	*DG*	1 1 1 1	SM	15.51 ± 0.06	13.61 ± 0.05	12.03 ± 0.18	1.34 ± 0.09	2.24 ± 0.17	0.90 ± 0.16	000	17	21	18
DZOA4662-04	1	14 00 10.9:	–59 12 35:	311.64	2.50	5.2	*UG*	0 1 1 0	SM/L	16.35 ± 0.11	... ...	... ...	... ...	... ...	... ...	000	5	8	...

Table 2. continued.

Ident.	N	RA (J2000) [h m s]	Dec [° ′ ″]	Gal ℓ [°]	Gal b [°]	A_B [mag]	Class	Visibil.	Type	I [mag]	J [mag]	K [mag]	$(I-J)^0$ [mag]	$(I-K)^0$ [mag]	$(J-K)^0$ [mag]	Phot.	D_I [″]	D_J [″]	D_K [″]
(1)	(2)	(3a)	(3b)	(4a)	(4b)	(5)	(6)	(7)	(8)	(9)	(10)	(11)	(12)	(13)	(14)	(15)	(16)	(17)	(18)
DZOA4662-07	1	14 00 26.9:	–60 18 31:	311.38	1.43	15.4	*UG*	0 0 1 1	?	... ...	14.37 ± 0.07	12.69 ± 0.15	... ...	... ...	0.16 ± 0.16	000	...	11	9
DZOA4663-05	2	14 00 33.9	–59 32 32	311.60	2.16	6.6	*DG*	0 1 1 1	SE/M	16.53 ± 0.07	12.86 ± 0.02	11.45 ± 0.08	1.37 ± 0.08	2.27 ± 0.09	0.90 ± 0.06	000	6	16	11
DZOA4663-02	1	14 00 55.3	–57 37 23	312.15	4.00	2.9	*DG*	0 1 1 0	SM	15.02 ± 0.03	14.22 ± 0.05	... ...	0.23 ± 0.06	... ...	... ...	000	13	15	...
DZOA4663-01	1	14 00 55.8	–57 37 28	312.15	4.00	2.9	*DG*	0 1 1 0	SM	15.27 ± 0.04	13.64 ± 0.04	... ...	0.74 ± 0.05	... ...	... ...	000	14	16	...
DZOA4663-04	1	14 01 25.6	–58 37 37	311.95	3.01	4.4	*DG*	0 1 1 1	SE/M	15.84 ± 0.07	13.43 ± 0.04	11.99 ± 0.10	1.11 ± 0.08	2.19 ± 0.14	1.08 ± 0.13	000	11	14	10
DZOA4663-03	1	14 01 35.4	–58 32 22	311.99	3.09	4.3	*UG*	0 1 1 0	S	16.38 ± 0.14	15.39 ± 0.20	... ...	0.04 ± 0.20	... ...	... ...	000	7	8	...
DZOA4664-02	1	14 03 11.2	–58 06 20	312.31	3.45	3.5	*DG*	0 1 1 1	SL	15.03 ± 0.05	13.46 ± 0.05	... ...	0.83 ± 0.09	... ...	... ...	000	15	15	6
DZOA4665-02	2	14 03 13.8	–58 07 13	312.31	3.44	3.6	*DG*	0 1 1 1	SM	14.50 ± 0.02	12.61 ± 0.02	11.67 ± 0.05	0.81 ± 0.03	1.66 ± 0.06	0.85 ± 0.06	030	18	21	12
DZOA4665-03	1	14 03 57.5	–58 09 49	312.40	3.37	4.0	*UG*	0 1 1 1	SM/L	... ...	... ...	... ...	... ...	... ...	... ...	000	8	15	6
DZOA4665-01	2	14 04 21.0	–57 43 33	312.57	3.77	2.9	*DG*	0 1 1 1	E	15.21 ± 0.03	13.29 ± 0.03	12.13 ± 0.10	1.10 ± 0.04	2.13 ± 0.06	1.03 ± 0.07	000	10	14	11
DZOA4666-01	1	14 05 35.9	–59 32 19	312.21	1.99	8.5	*UG*	0 1 1 1	SM/L	17.00 ± 0.16	14.70 ± 0.13	... ...	0.09 ± 0.16	... ...	... ...	000	6	12	5
B-band galaxies found to be non galaxian with DENIS:																			
DZOA4654-04	1	13 49 41.3	–57 48 40	310.65	4.18	2.6	*NG*	1 1 0 0	–	... ...	... ...	... ...	... ...	... ...	... ...	000	4	...	...
DZOA4655-07	1	13 50 51.8	–57 43 02	310.82	4.24	2.6	*NG*	1 1 1 0	–	... ...	... ...	... ...	... ...	... ...	... ...	000	5	4	...
DZOA4660-06	2	13 56 42.9	–59 11 16	311.22	2.63	5.1	*NG*	1 1 1 1	–	15.95 ± 0.05	14.62 ± 0.06	... ...	0.08 ± 0.11	... ...	... ...	000	...	...	...
DZOA4661-04	1	13 58 40.7	–58 18 13	311.69	3.42	3.5	*NG*	1 1 1 0	–	... ...	... ...	... ...	... ...	... ...	... ...	000	...	...	...
DZOA4664-03	2	14 02 42.0	–57 44 08	312.35	3.83	3.3	*NG*	1 1 0 0	–	... ...	... ...	... ...	... ...	... ...	... ...	000	...	...	...